ISSN 0256-4637
VOLUME 40 NUMBER 3 JULY-SEPTEMBER 2018

Journal of Pure and Applied

Ultrasonics

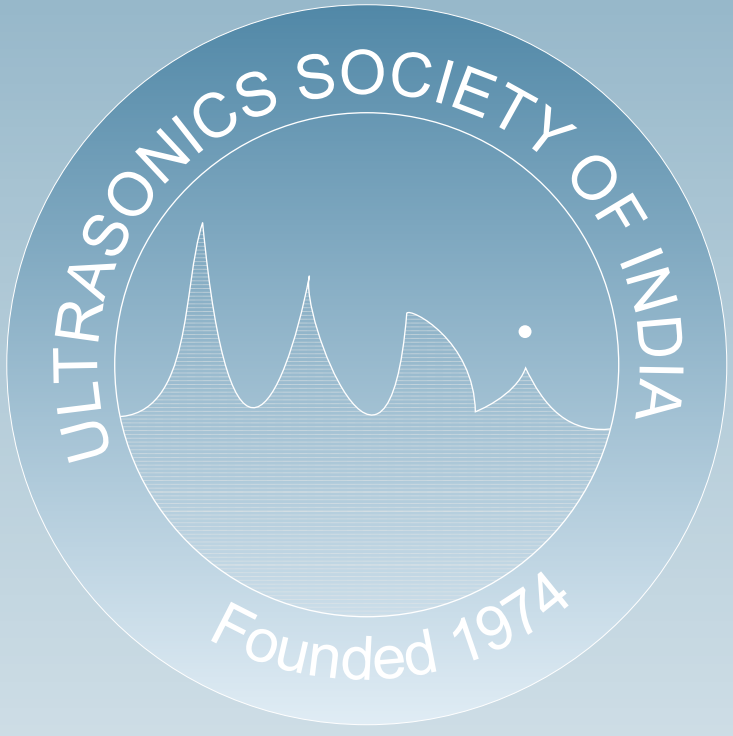

Website : www.ultrasonicsindia.org

A Publication of Ultrasonics Society of India

A Quarterly Publication of Ultrasonics Society of India

Journal of Pure and Applied

Ultrasonics

No. 3	Volume 40	July-September 2018

SUBSCRIPTION (postage paid)

Single	Rs. 750/-	US$ 60/-
Annual	Rs. 3000/-	US$ 250/-
USI *members*	Free	

The submission of papers and all other correspondence regarding the Journal may please be addressed to :

Publication Secretary
Journal of Pure and Applied Ultrasonics
C/o Ultrasonics Society of India
CSIR-National Physical Laboratory
Dr. K.S. Krishnan Road, New Delhi-110012
publicationsecretary.usi@gmail.com
www.ultrasonicsindia.org

ISSN 0256–4637

Journal of Pure and Applied Ultrasonics

VOLUME 40 NUMBER 3 JULY–SEPTEMBER 2018

CONTENTS

(Authors have stated that the papers have not been published elsewhere)

Website : www.ultrasonicsindia.org

A Publication of — Ultrasonics Society of India

J. Pure Appl. Ultrason. 40 (2018) pp. 63-72

Divergence controlled ultrasonic array for 3-D imaging

Sahdev Kumar* and Hideo Furuhashi

Department of Electrical and Electronics Engineering, Aichi Institute of Technology,
Toyota, 1247 Yachigusa, Yakusa-Cho, Toyota, 470-0392, Japan
*E-mail: kumarsahdev42@gmail.com

In this paper we present the experimental studies on characteristics of isotropic divergence controlled ultrasonic phased array transmitter (PAT) with wide field-of-view in range sensing and imaging. In earlier theoretical and experimental investigations it was demonstrated that a long range sensor and imaging system is feasible with an increased high power of an ultrasonic array transmitter just by increasing a number of ultrasonic transmitter elements. An increase in the range sensing abilities of a high power ultrasonic PAT, however, limits its field-of-view angle up to a few degrees as compared to the conventional range imaging method due to high directionality through beam formation. Thus, any improvement in the field-of-view angle requires a divergence control of an ultrasonic PAT by controlling the delay-time of 40 kHz signal modulated as pulse of 2 ms for each element. We, successfully characterized isotropic divergence controlled ultrasonic PAT to compare our experimental results with the theoretical simulations. An object detection field-of-view angle of 18° has been confirmed at the divergence angle of 20° by our ultrasonic PAT with relatively reduced range imaging, which was still higher than that of a range measurement reported by conventional ultrasonic system. In this paper we have considered a simple isotropic divergence controlled ultrasonic PAT for wider field-of-view in range sensing.

Keywords: 3-D range sensing system, ultrasonic phased array transmitter, isotropic divergence, delay-time.

Introduction

Ultrasonic sensing, imaging, and measurement technologies have attracted considerably increased attention by playing significant role in last several decades with its applications in robotics, amusement, security, presence sensing, material characterization and biomedical imaging *etc*. A relatively higher directionality along with its transmission characteristics through the solids, liquids, and gaseous medium makes it an indispensable versatile tool for a large number of industrial use. A 3-dimensional shape and size measurement of an object in air, using ultrasonic technology were also considered[1-3]. Although, there are other techniques available for 3D position and shape recognition such as stereo camera, laser scanner, pattern projection *etc*. Ultrasonic imaging system provides a simple and cost effective optional technique that produces the shape and range image of an ultrasonic reflecting object employing the delay-and-sum (DAS) operations[4-7]. In spite of its low resolution with short measurable range in air, ultrasonic technology remained indispensable owing to its effective use in adverse atmospheric conditions such as darkness, rain, fog, smoke *etc*. The inter-element space in a receiver array can be reduced using micro electromechanical system (MEMS) arrays in a single chip for higher resolution and wider field-of-view (FOV)[6,7]. A compact and reduced size receiver array was also reported using lead zirconate titanate (PZT) thin films[8,9].

We reported a novel ultrasonic range imaging system with 2-dimensional high power ultrasonic PAT using 144 transmitting elements in the form of (12×12) square matrix and a receiver array consisting of 32 receivers[10,11]. Owing to the beam formation characteristics of an ultrasonic PAT, that generates highly directional signal but reduces FOV angle[12,13]. Therefore, to improve FOV, a divergence control on

directivity has been proposed and our theoretical simulation results shown that measurement field increases with an increase in divergence but reduces the measurable range accordingly[12]. We, clarified these problems through our theoretical and experimental studies on PAT for FOV and range sensing improvements[12-14]. In this study, an isotropic divergence controlled ultrasonic transmission system was characterized for 3-D measurement of an object to improve the FOV. In which, equal time-delay was applied for both *x* and *y* plane of PAT to simplify the system operation. The experimental and theoretical characterization of our ultrasonic PAT for different isotropic divergence angles have shown considerable improvement in FOV.

Theory

Figure 1 depicts a coordinate system of divergence calculation.

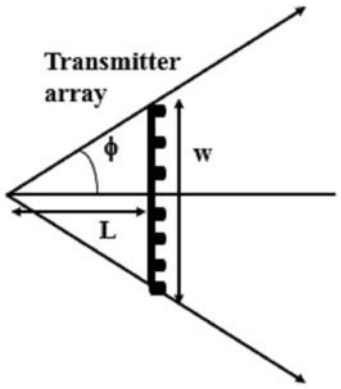

Fig. 1. Coordinate system of divergence control.

When an ultrasonic sound source was considered to be located behind an array on line *L*, a divergence angle ϕ is calculated by Eq. (1)[12]

$$\tan\phi = \frac{w}{2L} = \frac{(N-1)d}{2L} \tag{1}$$

Here, *N* is the number of rows of transmitting elements in PAT and *d* is inter-element spacing.

The time delay between sound waves at the origin (0, 0) and the position of an element (x_i, y_i) was calculated by Eq. (2)[12]

$$\Delta\tau_d = \frac{\Delta L}{\nu} = \frac{x_i^2 + y_i^2 + L^2 - L}{\nu} \approx (x_i^2 + y_i^2)\frac{2}{2L\nu} \tag{2}$$

Here, ΔL is a distance between ultrasonic source elements and *v* as the wave velocity.

The phase difference was calculated on the basis of a time-delay using Eq. (3)[12]

$$\Delta\varnothing = 2\pi\frac{\nu\Delta\tau_d}{\lambda} = 2\pi(x_i^2 + y_i^i)\frac{1}{2L\lambda} \tag{3}$$

The ultrasonic sound pressure at point *P(x, y, z)* was calculated using Eq. (4)[12]

$$p(x,y,z) = \sum_i D(\theta_i)A_i\frac{e - 2\pi i\frac{r_i + \nu\Delta\tau_d}{\lambda}}{r_i} \tag{4}$$

Here, r_i is a distance between positions P_i of the elements and the observation point *P(x, y, z)*, θ_i is an angle between the *z* axis and the vector P*i*P, D(θ_i) is the directivity of each element and A_i is the amplitude. If observation point *P* is sufficiently far from the origin in comparison to the size of the transmitter array then Eq. (4) may be extended as Eq. (5)[12]

$$\begin{aligned}\left|p(x,y,z)\right| &= D(\theta)A\frac{1}{r}\sum_{i=1}^{n}\exp\left|\left\{-i\frac{2\pi}{\lambda}(x_i\sin\theta_x + y_i\sin\theta_y + \frac{x_i^2+y_i^2}{2L}\right\}\right| \\ &= D(\theta)A\frac{1}{r}\sum_{i=1}^{n}\exp\left|\left\{-i\frac{2\pi}{\lambda}(x_i\sin\theta_x + y_i\sin\theta_y + \frac{x_i^2+y_i^2}{(n-1)d}\tan\phi\right\}\right|\end{aligned} \tag{5}$$

It is assumed that all transmitting elements have the same sound pressure amplitude.

Ultrasonic Transmitting and Receiving system

Ultrasonic phased array transmitting system

Figure 2 shows a photograph of the developed ultrasonic PAT consisting of 144 transmitter elements in the form of square matrix (12 × 12) using device T4010B4 with the inter-element spacing of 1cm. Figure 3 shows the schematic block diagram of ultrasonic PAT system. An applied signal to each transducer element was controlled by FGPA (XILINXXC6SLX150) boards with a 50 MHz clock signal in the form of modulated signal. A 40 kHz signal was modulated in the form of 2 ms pulse width with 400 ms pulse repetition period and stored in a ring buffer. There were total four FPGAs one of them was used as the master board to feed the amplitude-modulated digital signal to the other three slave boards. The time-delays (rounded off to 1 μs) were calculated according to the applied divergence by a personal computer using Eq. (2) and sent to the FPGAs board. The delayed signals were converted from digital to analogue by D/A convertors AD5415 (a 12-bit, dual-channel) at a sampling rate of 1 μs. The generated signals with the equal amplification factor were sent to the transmitter for transmission[13].

Fig. 2. A photograph of developed PAT.

Figure 3 shows the schematic block diagram of ultrasonic PAT system.

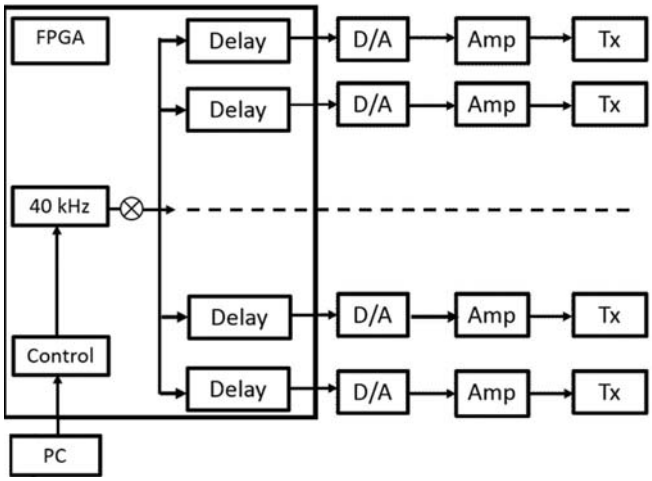

Fig. 3. Schematic block diagram of the ultrasonic transmitting system.

An applied signal to each transducer element was controlled by FGPA (XILINXXC6SLX150) boards with a 50 MHz clock signal in the form of modulated signal. A 40 kHz signal was modulated in the form of 2 ms pulse width with 400 ms pulse repetition period and stored in a ring buffer. There were total four FPGAs one of them was used as the master board to feed the amplitude-modulated digital signal to the other three slave boards. The time-delays (rounded off to 1 μs) were calculated according to the applied divergence by a personal computer using Eq. (2) and sent to the FPGAs board. The delayed signals were converted from digital to analogue by D/A convertors AD5415 (a 12-bit, dual-channel) at a sampling rate of 1 μs. The generated signals with the equal amplification factor were sent to the transmitter for transmission[13].

Ultrasonic receiving system

The ultrasonic receiving system consisting of 32 omni-directional SP0103NC3-3 (6.15 mm (length) x 3.76 mm (width) x 1.45 mm (height) elements. Figure 4 shows the schematic block diagram of the receiving system.

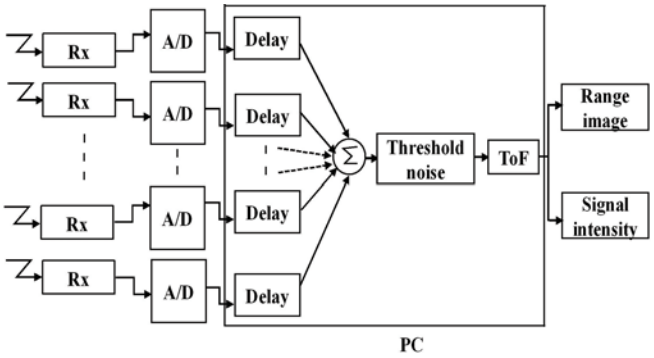

Fig. 4. Schematic block diagram of the ultrasonic receiving system.

The 40 kHz generated signal by the PAT was received after its reflection from a plastic board (30 cm width x 80 cm length). An A/D convertor TSM-372012 (Interface Corporation) was used to convert the received analogue signal into digital form. The signal conversion time from analog to digital was 2.5 μs with a 12 bits resolution. The output of hardware system shows range image and signal intensity of the target object after signal processing (DAS operations) using MATLAB and Simulink[13].

Experimental Set-up

The transmitted signal was received by a sensor in the horizontal plane facing towards each other as depicted in Fig. 5.

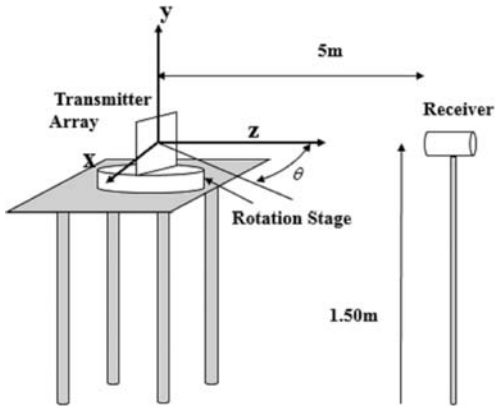

Fig. 5. Experimental Setup

The sensor was placed at 5 m from PAT at the height of 1.5 m above the ground level. The sensor was calibrated at the ultrasonic frequency by a system using a ¼-inch free-field response microphone (46BE; frequency range 4 Hz-80 kHz, dynamic range 36 dB-157 dB, G.R.A.S Sound and Vibration A/S), a data acquisition module (USB-4431; 24-Bit Analog I/O, sampling rate of 102.4 kS/s, National Instrument Corp.), and a sound measurement analyzer (NI Sound and Vibration Measurement Suite; National Instrument Corp.)[13]. A device MA40S4R (Murata Co. Ltd), was used as a sensor which has a nominal frequency of 40 kHz and beam width of 80°. At first, experiment was initialized by obtaining the maximum amplitude of the directly received signal with the set parameters, then divergences were input through personal computer and time-delay was calculated by the system accordingly. The Vpp was measured by rotating the PAT on the azimuthal angle in *z* direction from 0°-90° at 2° steps.

Experimental Results

Sound pressure level as a function of divergence angle

In this experiment $\sin\theta_x x_i + \sin\theta_y y_i = 0$ was considered and on the *z* axis (θ_x = 0° and θ_y = 0°) according to Eq. (5) without divergence control ϕ = 0° the sound pressure level 126 dB has been reported at 5 m distance from the transmitter[13, 14]. The sound pressure level was obtained 122.3 dB, 119.8 dB and 110.6 dB at 5 m from the array Tx for applied divergences ϕ = 10°, 20° and 30°, respectively. Figure 6 shows the dependence of sound pressure level as a function of divergence angle.

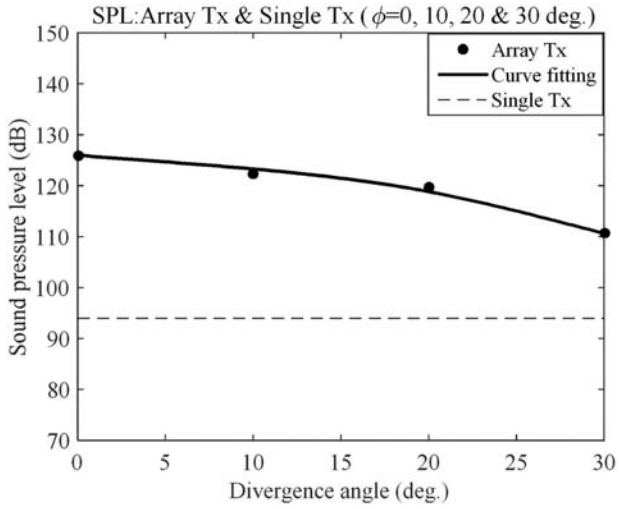

Fig. 6. Sound pressure level at divergence ϕ =0°, 10°, 20° and 30° (Array Tx vs Single Rx).

Divergence controlled directivities

Figures 7 (a)-(d) show the directivities of the array Tx with divergence control ϕ = 0°, 10°, 20° and 30°, accordingly.

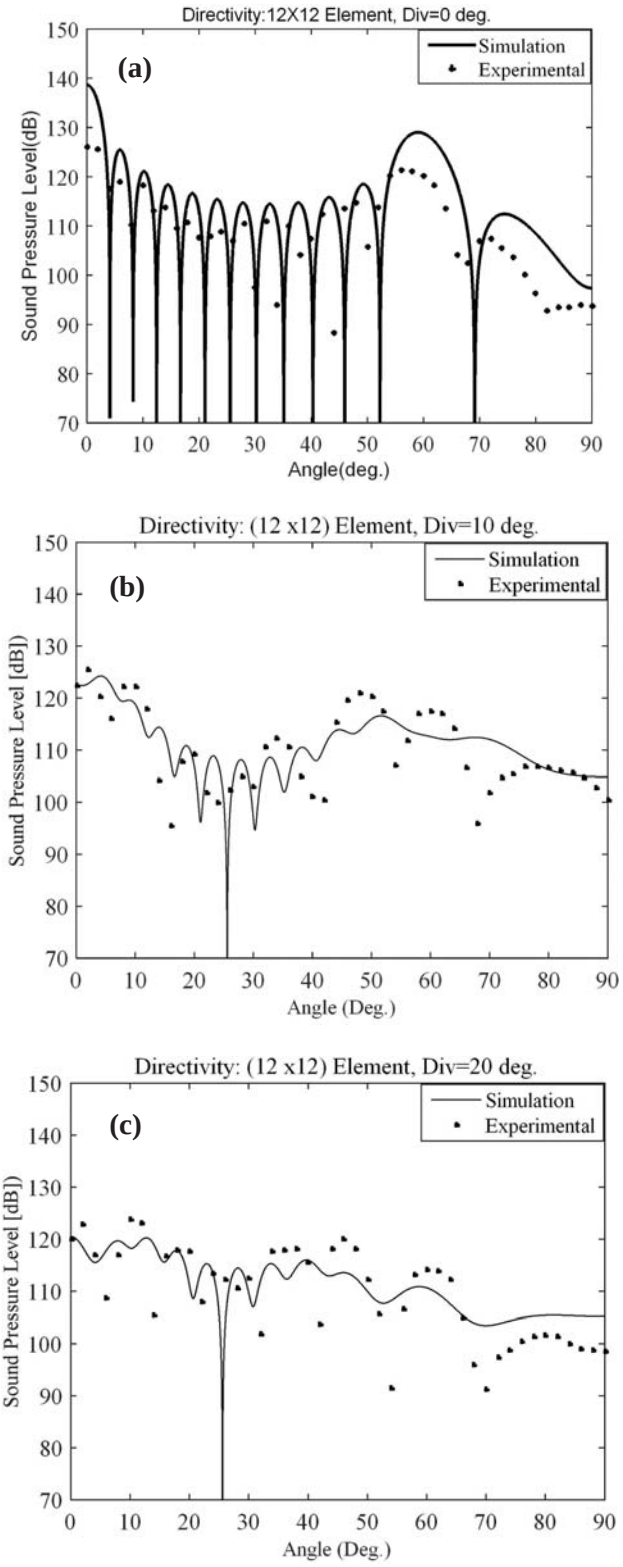

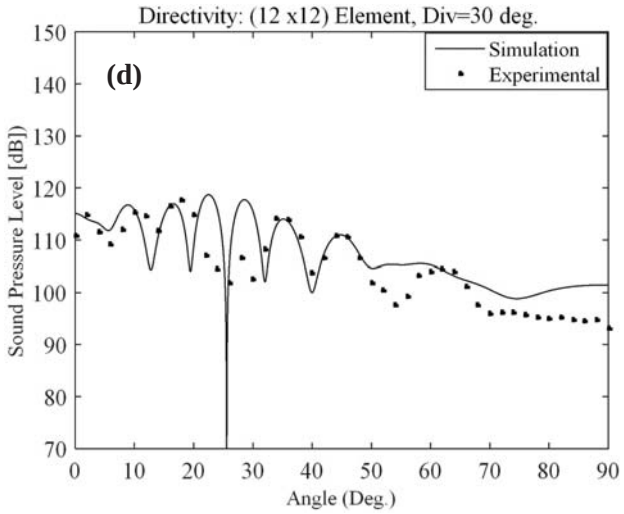

Fig. 7. Experimental and theoretical directivities
(a) Divergence $\phi = 0°$
(b) Divergence $\phi = 10°$
(c) Divergence $\phi = 20°$
(d) Divergence $\phi = 30°$

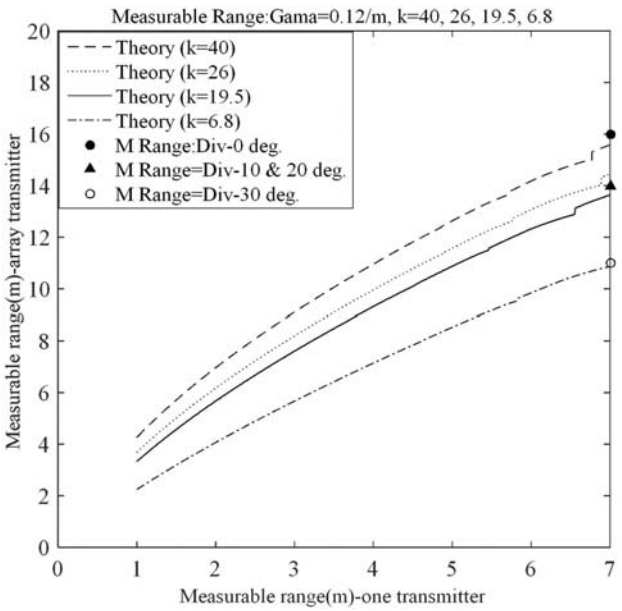

Fig. 8. Measurable range: at $\phi = 0°$, 10°, 20° and 30° using array Tx and single Rx.

The smooth line and dots represent the simulation and the experimental results, respectively. The time-delay was rounded off 1 μs and accordingly the resolution of the image was picked up by the system using Eq. (2). The directivities obtained by the experimental results were in good agreement with the simulation results. The divergence angles $\phi = 10°$, 20° and 30° were successfully controlled by the time-delay control of the developed system.

Measurable range

The measurable range of the array Tx with single Rx was calculated using the Eq. (6)[10-14].

$$\frac{e^{-2\gamma r'}}{r'^2} = k\frac{e^{-2\gamma r''}}{r''^2} \qquad (6)$$

Here, k is the ratio of transmitted sound pressure of the array Tx to that of single Tx and calculated as 40, 26, 19.5 and 6.8 with the divergence angles $\phi = 0°$, 10°, 20° and 30°, respectively. The measurable ranges of single Tx and array Tx were denoted by r' and r''.

Figure 8 shows the measurable range using array Tx and single Rx.

The measurable range without divergence control ($\phi = 0°$) was obtained 16 $\pm$ 0.5 m. The measurable ranges for divergence $\phi = 10°$, 20°, and 30° were obtained as 14 $\pm$ 0.5 m, 14 $\pm$ 0.5 m, and 11 $\pm$ 0.5 m, respectively and denoted by black circle, black triangle and circle accordingly for a plastic reflection board (30 cm width × 80 cm height). The theoretical measurable ranges calculated with k = 40, 26, 19.5 and 6.8 were denoted by dashed, dotted, solid and dash-dotted lines, respectively. These theoretical calculations were made using absorption coefficient γ = 0.12/m in Eq. (6)[14].

Object detection view angle

Figure 9 shows the dependence of view angle on the measurable range with respect to divergence angle in the direction $\phi_x = \phi_y = 0°$.

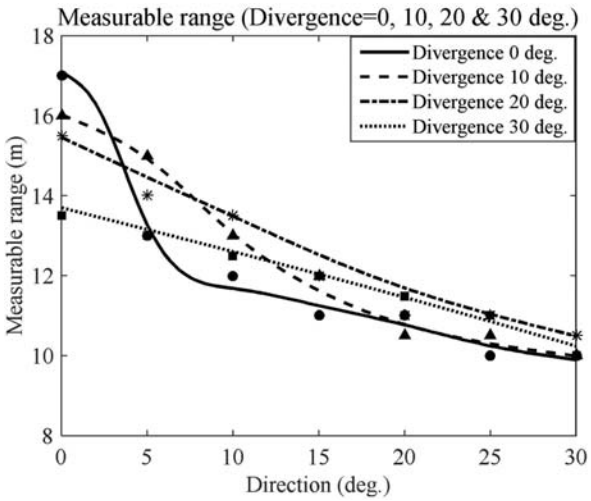

Fig. 9. Object detection view angle at different measurable range with $\phi = 0°$, 10°, 20° and 30° using array Tx and array Rx.

The object detection view angle using array Tx and array Rx with divergence control was probed using a hard board reflector (12 cm width × 15 cm height × 4 cm depth). The measurable range becomes shorter with the increased divergence angle and the slope of the curves become more and more smooth. The view angles at the measurable range 12 m were 5°, 13°, 18° and 15° (half width) for the divergence control angle ϕ = 0°, 10°, 20° and 30°, respectively. The theoretical results were denoted by solid, dashed, dash-dotted, and dotted lines. The experimental results were shown by circles, triangles, stars and squares, respectively. Although the measurable range of the array Tx with array Rx without divergence control was 17 $\pm$ 0.5 m. The widest FOV angle 18° has been obtained at the divergence angle =20°.

Obtaining range image of an object

Figures 10(a) - 13(a) show the range images of a plastic board (30 cm width × 80 cm height) located at 11 m in the direction θ = 0° from transceiver, applying the divergence ϕ = 0°, 10°, 20° and 30°.

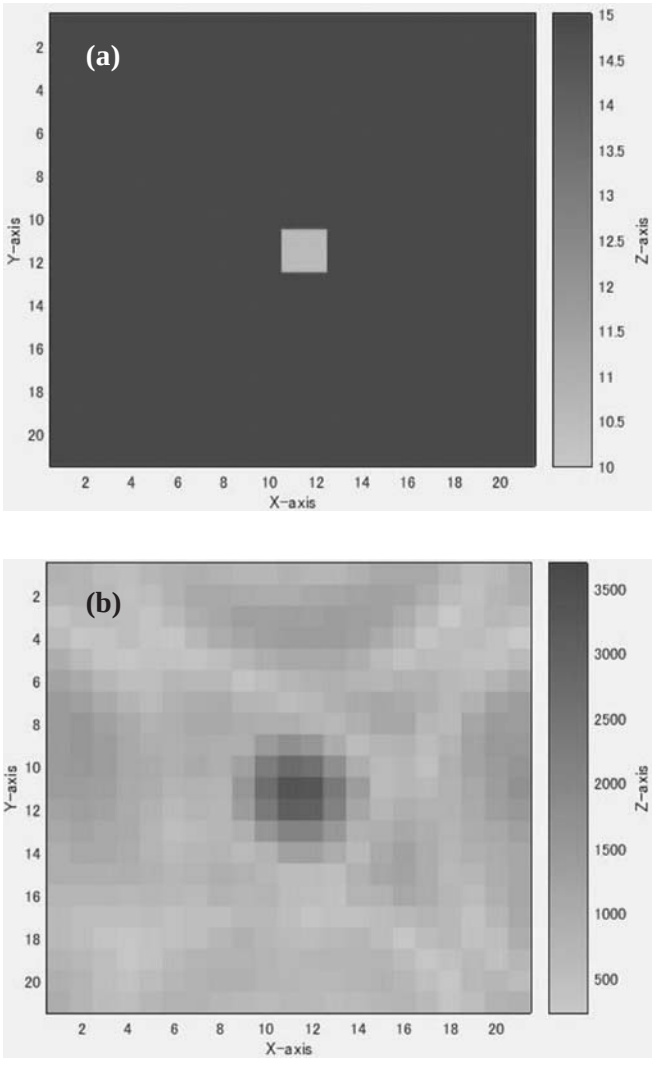

Fig. 10. Range image and signal intensity after delay-and-sum operations. The object is 11 m in θ = 0° direction from transreceiver and applied divergence ϕ = 0°; *x* and *y* axis are 5°/div and *z* axis shows the distance between the transceiver and the object.
(a) Range Image
(b) Signal Intensity

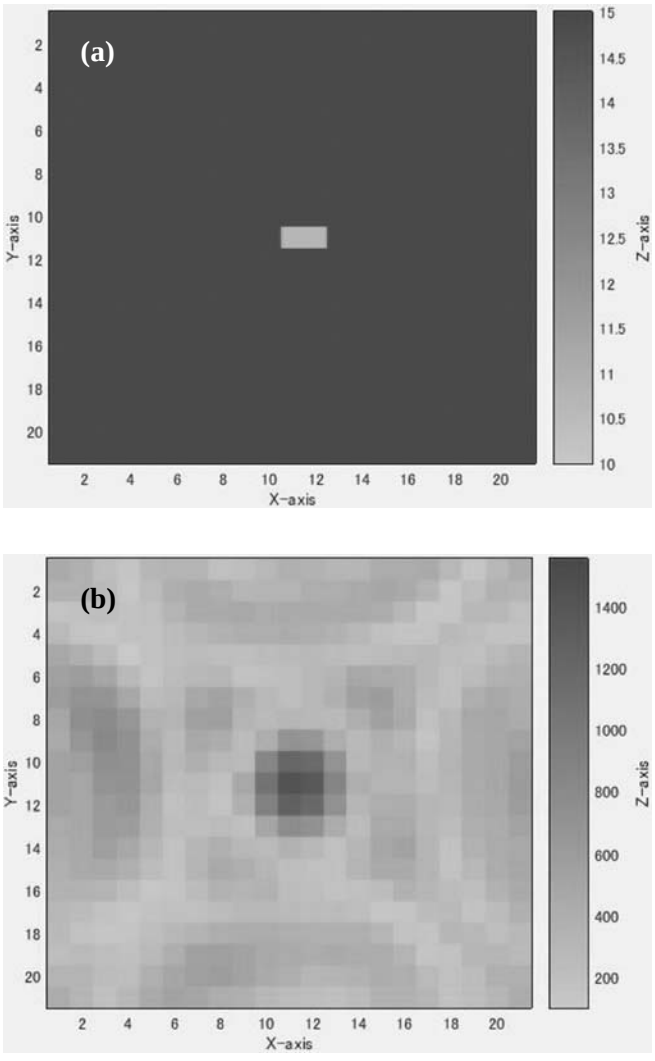

Fig. 11. Range image and signal intensity after delay-and-sum operations. The object is 11 m in θ = 0° direction from transreceiver and applied divergence ϕ = 10°, *x* and *y* axis are 5°/div and *z* axis shows the distance between transceiver and object.
(a) Range Image
(b) Signal Intensity

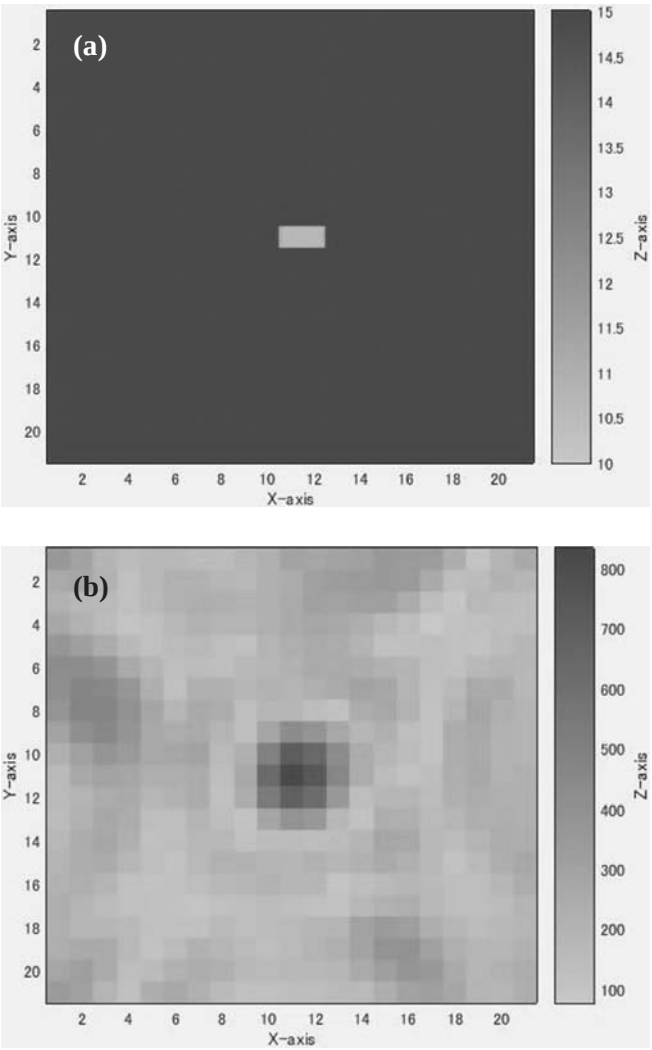

Fig. 12. Range image and signal intensity after delay-and-sum operations. The object is 11 m in θ = 0° direction from transreceiver and applied divergence ϕ = 20°, *x* and *y* axis are 5°/div and *z* axis shows the distance between transceiver and object.
(a) Range Image; (b) Signal Intensity

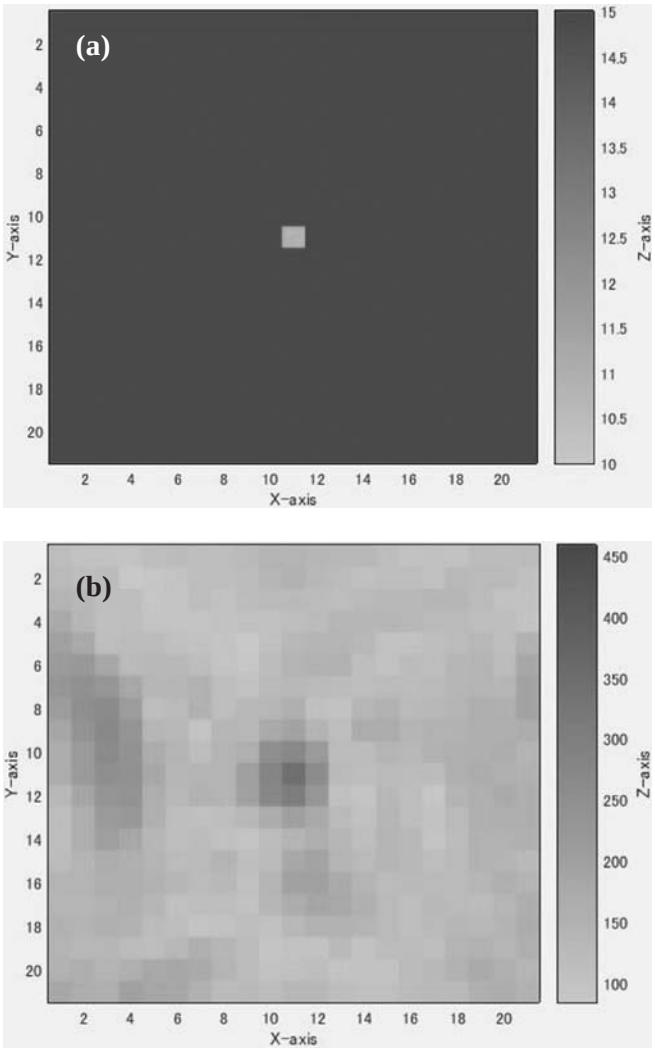

Fig. 13. Range image and signal intensity after delay-and-sum operations. The object is 11 m in θ = 0o direction from transreceiver and applied divergence ϕ = 30°, *x* and *y* axis are 5°/div and *z* axis shows the distance between transceiver and object.
(a) Range Image; (b) Signal Intensity

Figures 10(b) - 13(b) show the respective signal intensity of their range images. Figure 14 shows the dependence of signal intensity with respect to divergence angle.

The signal intensity decreases significantly as divergence angle increases and reduced to one forth from divergence $\phi = 0°$ to $\phi = 10°$. Further, signal intensity becomes half at divergence $\phi = 20°$ in comparison of =10o and continued to decrease with divergence increase. The range image of the target object was clearly detected locating the object at different positions and applying different divergence angles.

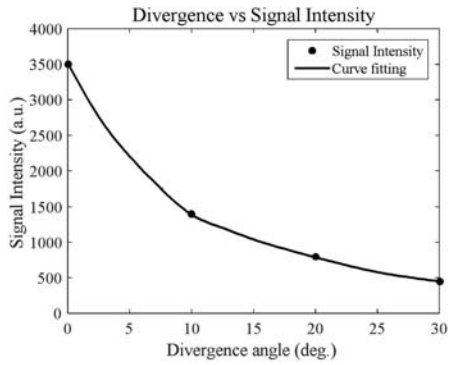

Fig. 14. Dependence of signal intensity as a function of divergence angle ϕ = 0°, 10°, 20° and 30°.

Figure 15(a) shows the range image of the object locating it in the θ = 10° direction and applying divergence angle ϕ = 10°. Figure 15(b) shows the respective signal intensity of that range image. Figure 16(a) shows the range image of the object locating in θ = 20° direction and applying divergence angle θ = 20°. Figure 16 (b) shows the respective signal intensity of that range image. Similarly, Figure 17(a) shows the range image of the object locating it in the θ = 20° direction and applying divergence angle ϕ = 30°. Figure 17(b) shows the respective signal intensity of that range image. The object has been detected successfully in the directions it was located.

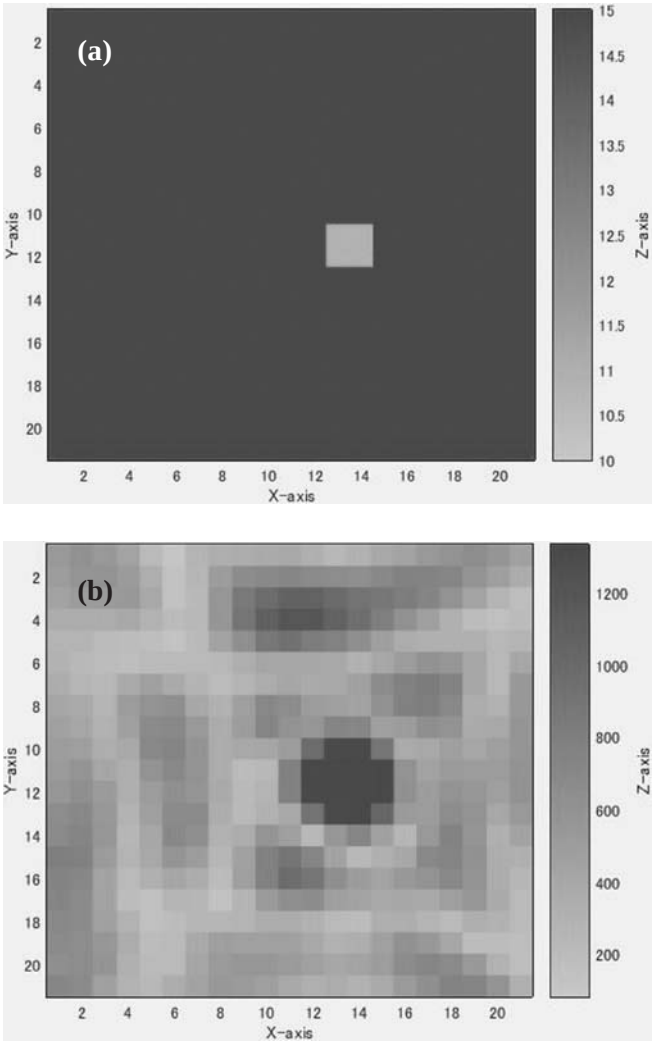

Fig. 15. Range image and signal intensity after delay-and-sum operations. The object is 11 m in θ = 10° direction from transreceiver and applied divergence ϕ = 10°, *x* and *y* axis are 5°/div and *z* axis shows the distance between transceiver and object.
(a) Range Image; (b) Signal Intensity

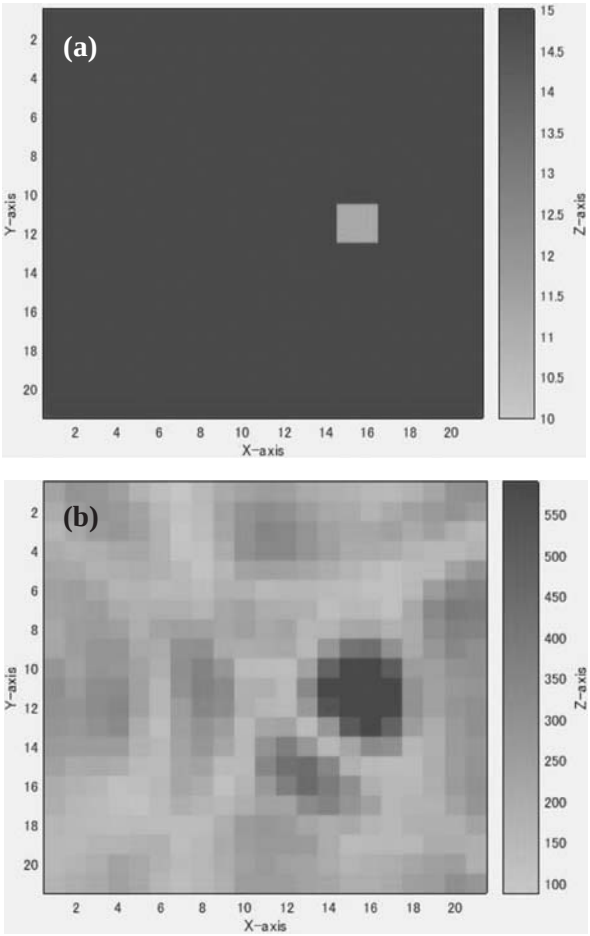

Fig. 16. Range image and signal intensity after delay-and-sum operations. The object is 11 m in θ = 20° direction from transreceiver and applied divergence ϕ = 20°, *x* & *y* axis are 5°/div and *z* axis shows the distance between transceiver and object.
(a) Range Image; (b) Signal Intensity

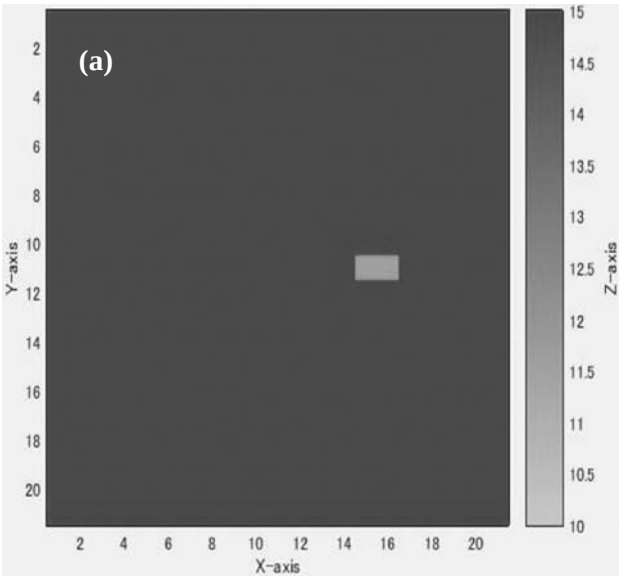

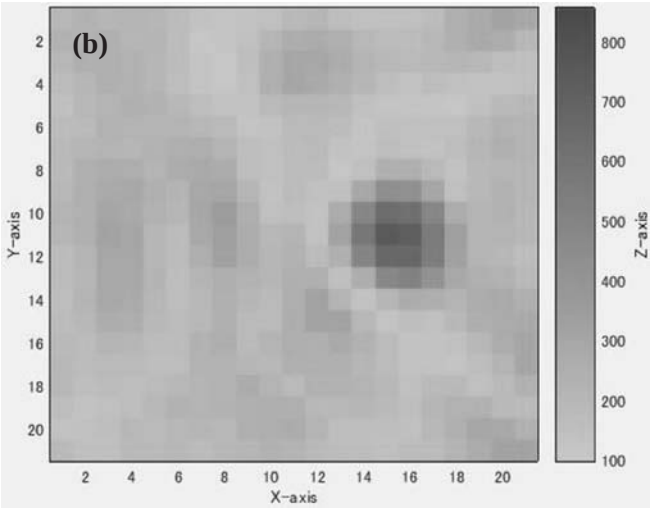

Fig. 17. Range image and signal intensity after delay-and-sum operations. The object is 11 m in θ = 20° direction from transreceiver and applied divergence ϕ = 30°, *x* and *y* axis are 5°/div and *z* axis shows the distance between transceiver and object.
(a) Range Image; (b) Signal Intensity

Detection of position of the object

The signal intensity and the range images were displayed in 21 × 21 pixels constructed using MATLAB and Simulink. The maximum signal intensity distribution and range image data were calculated when the correlated signal reached to its maximum value. The total field of view angle of the ultrasonic array Rx in *x* and *y* directions was 105° × 105°. An object placed at 11 m in the direction =0o from the transceiver and, its range image detected at the center position of the 21 × 21 pixels as given by $\left(0°\times\frac{21\ pixeis}{105\ deg.}+\frac{21\ pixeis}{2}=11^{th}\ pixel\right)$ Pixel point (11, 11) has been the center and its coordinates were considered as (0, 0). The range images were successfully obtained at the center when $\theta = 0°$ and $\phi = 0°$, 10°, 20° and 30° as shown in Figs. 10(a)-13(a); *z* axis shows the distance between transmitter and object through the color match. The position of the object located at 11 m in $\theta = 0°$ can be written as (0°, 0°, 11 m). The angular view resolution 5°/pixel and range image of the object was detected at (0 pixel, 0 pixel, 11.5 m), that represents the measured position as (0°, 0°, 11.5 m) for all the four cases. Figures 10(b)-13(b) show the respective signal intensities.

Further, an object located at 11 m in the direction $\theta =$ 10° and 20°, its range images were expected to be 2 pixels and 4 pixels sifted from the center position of the 21×21 pixels as calculated by $\left(10°\times\frac{21\ pixeis}{105°}+\frac{21\ pixeis}{2}=13^{th}\ pixel\right)$ and $\left(20°\times\frac{21\ pixeis}{105°}+\frac{21\ pixeis}{2}=15^{th}\ pixel\right)$. The pixel point were obtained as (13, 11) and (15, 11). The positions of the object can be written as (10°, 0°, 11 m) and (20°, 0°, 11 m). The angular view resolution 5°/pixel and range images of the object were detected at (2 pixel, 0 pixel, 11.5 m) and (4 pixel, 0 pixel, 11.5 m), that represent the measured positions as (10°, 0°, 11.5 m) and (20°, 0°, 11.5 m). Figures 15(a) and 16(a) show the measured position of the target object at divergence angles ϕ = 10° and 20°. Figures 15(b) and 16(b) show the respective signal intensities. Similarly, an object located at 11 m in the direction θ =20° and divergence angle ϕ = 30°, its range image was expected 4 pixels sifted from the center position. The position of the object can be written as (20°, 0°, 11 m) and its range image was detected at (4 pixel, 0 pixel, 11.5 m) that represents the measured position as (20°, 0°, 11.5 m). Figures 17(a) and (b) show the range image of the object and its respective signal intensity. The measurement error was considered (1×1) pixel for the variation in the view angle of 5° and range image resolution depends on the pulse width, pulse speed, distance and size of the object. It becomes as $\Delta z=\left(\frac{Pulse\ width(s)\times Wave\ velocity(m/s)}{2}\right)+$ position error(m) = 0.55 m for a pulse width 2 ms, ultrasonic wave speed 345 m/s and object positioning error 0.20 m and it was in agreement within experimental error of ± 0.50 m.

Conclusions

A three dimensional range sensing system has been developed using an ultrasonic PAT and an array Rx. The divergence ϕ = 10°, 20° and 30° of the array Tx is successfully controlled by the delay-time control of each transmitting element. The FOV becomes wider with the increased divergence angle. The widest FOV angle was obtained at divergence angle ϕ = 20°. The peak sound pressure decreased with an increase in the divergence angle and resulted in shorter measurable range. The experimental results were found in good agreement with the theoretical simulations.

Acknowledgements

One of the authors (S. Kumar) thankfully acknowledges the financial support received from Rotary Yoneyama Memorial Foundation Fellowship, Japan. The

technical assistance in the experiments by Miss Aishwarya Singh and useful discussions on electronic control circuits with Prof. Yoshiyuki Uchida, Prof. Masakazu Mori, Prof. Norio Tsuda and Dr. Brahm Pal Singh are gratefully acknowledged.

References

1 **Turnbull D.H.** and **Foster F.S.**, Beam Steering with Pulsed Two-Dimensional Transducer Arrays, *IEEE Trans. Ultrason., Ferroelectr., Freq.Control,* **38**(4) (1991) 320-333.

2 **Beardsley B., Peterson M.** and **Achenbach J.D.**, A simple scheme for self-focusing of an array, *J. Nondestr. Eval*. **14**(4) (1995) 169-179.

3 **Azar L., Shi Y.** and **Wooh S.C.**, Beam focusing behavior of linear phased arrays, *NDT E Int.* **33**(3) (2000) 189-198.

4 **Zhu H., Inubushi H., Takahashi N.** and **Taniguchi K.**, An ultrasonic 3D image sensor employing PN code, Sensors. *IEEE* (2006) 319-322.

5 **Harput S.** and **Bozkurt A.**, Ultrasonic phased array device for acoustic imaging in air, *IEEE Sensors J.* **8**(11) (2008) 1755-1762.

6 **Harput S., Bozkurt A.** and **Yamaner F.Y.**, Ultrasonic phased array device for real-time acoustic imaging in air, *IEEE Proc. Intl. Ultrasonics Symposium,* (2008) 619-622. DOI:10.1109/ULTSYM.2008.0148.

7 **Przybyla R.J., Shelton S.E., Guedes A., Krigel R., Horsley D.A.** and **Boser B.E.**, In-air ultrasonic range finding and angle estimation using an array of AlN micromachined transducers, *IEEE Sensors, J.,* **11**(11) (2011) 2690-2697.

8 **Yamashita K., Chansomphou L., Murakami H.** and **Okuyama M.**, Ultrasonic micro-array sensors using piezoelectric thin films and resonant frequency tuning, *Sensors and Actuators, A,* **114**(2) (2004) 147-152.

9 **Yamashita K., Murakami H., Okuyama M., Tanaka T., Mo Y., Suzuki Y.** and **Arita S.**, Ultrasonic phased-array sensor using PZT thin film and three-dimensional object detection using BBD, *J. Korean Phys. Soc.,* **42** (2003) S1108-S1112.

10 **Kumar S., Ichi K.** and **Furuhashi H.**, Theoretical investiga-tion of high-power ultrasonic array transmitter for a range sensor in air, *Proc. IEEE, Int. conf. on industrial techno-logy ICIT 2013, IEEE Xplore* 2013, (2013) 1190-1195.

11 **Kumar S., Wei Q.** and **Furuhashi H.**, Characteristics of High-Power ultrasonic array transmitter in air, *Proc. IEEE 2015, Int. conf. on recent developments in control, automation and power engineering (RDCAPE 2015),* (2015) 209-213.

12 **Kumar S., Ichi K.** and **Furuhashi H.**, Theoretical investigation of divergence control of directivity of an ultrasonic transmitter array, *SICE annual conf.* 2013, Abstract SuCT2.1 2013, (2013) 803-807.

13 **Kumar S.** and **Furuhashi H.**, Anisotropic divergence controlled ultrasonic transmitter array for three-dimensional range imaging, *J. Pure Appl. Ultrason,* **38** (2016) 49-57.

14 **Kumar S.** and **Furuhashi H.**, Long-range measurement system using ultrasonic range sensor with high-power transmitter array in air, *Ultrasonics,* **74** (2017) 186-195.

J. Pure Appl. Ultrason. 40 (2018) pp. 73-79

Ultrasonic investigations of metal chlorides in aqueous ethanol systems

Bidyadhar Swain[1,*], Rabindra N. Mishra[2] and Upendra N. Dash[3]

[1]Department of Physics, DRIEMS, Cuttack-754022, India
[2]PG Department of Physics, Ravenshaw University, Cuttack-753003, India
[3]Plot No.436, Chakeisihani, Bhubaneshwar-751010, India
*E-mail: bidya.swain11@gmail.com

The density (d), ultrasonic velocity (U) and viscosity (?) measurements have been carried out for strong electrolytes, e.g., magnesium chloride and zinc chloride in 5, 10 and 15 wt% of aqueous ethanol in different concentrations over the temperature range 298.15K to 313.15K at 5K interval. Various thermo-acoustical parameters, such as free volume (V_f), internal pressure (π_i), relaxation time (τ), Gibb's free energy change (ΔG), ultrasonic attenuation (α/f^2) and van der Walls constant (b) have been computed from the experimental data to investigate the ion-solvent and solvent-solvent interactions in these systems. The variation of these parameters has been discussed and interpreted in the light of molecular interaction and hydrogen bonding in the solutions.

Keywords: Free volume, relaxation time, Gibb's free energy change,ultrasonic attenuation.

Introduction

Ultrasonic wave propagation through liquid systems and solids is now well established as an effective means of examining certain physical properties of the materials. Ultrasonic studies are widely employed to assess the thermo-acoustic properties and predict the intermolecular interactions in the liquid mixture and ionic interactions in electrolytic solutions[1,2]. Ultrasonic velocity together with density, viscosity and related acoustic parameters of electrolytes in mixed solvent systems assist in characterizing the structure and physical properties of solutions. The investigation of ultrasonic velocity and thermo-acoustic properties of electrolytes in aqueous and mixed solvent system has been the area of interest of many researchers[3,4]. So the study of intermolecular interaction plays a vital role in the development of molecular sciences.

In continuation of our earlier work in aqueous medium[5], the present investigation deals with the study of molecular interactions of strong electrolytes (magnesium chloride and zinc chloride) in 5, 10 and 15 wt% aqueous ethanol solvent systems in different concentrations over the temperature range 298.15K to 313.15K at 5K interval. Various thermo-acoustical parameters, such as free volume *(V_f)*, internal pressure *(π_i)*, relaxation time *(τ)*, Gibb's free energy change *(ΔG)*, ultrasonic attenuation *(α/f^2)* and van der Walls constant *(b)* have been computed from ultrasonic velocity *(U)*, density *(d)* and viscosity *(η)* data which provide qualitative information regarding nature and strength of the molecular interactions in the electrolytic solutions. The chemicals used in the work have wide applications in pharmacology, immunology, medicine and industry.

Experimental

Materials and Method

All electrolytes like magnesium chloride and zinc chloride used were of GR or AR grades obtained from Merck and dried over anhydrous $CaCl_2$ in desiccator before use. Ethanol from Merck with purity $\geq$ 99.9% was dehydrated by 4A molecular sieve and used. Conductivity water (Sp. cond. ~10^{-6} $S.cm^{-1}$) was used for preparing water + ethanol (5, 10 and 15 wt %) mixtures. The ethanol content in the mixed solvents was

accurate within ±0.01%. The solutions were prepared on the molal basis and conversion of molality to molarity was done by using standard expression[6] using the density data at the corresponding temperature. The solute content of the solutions varied over a concentration range of 6.0 × 10^{-3} M to 8.0 × 10^{-2} M for all measurements.

Velocity measurement

Ultrasonic velocity measurements in the solutions were made by using a multi frequency ultrasonic interferometer operating at a frequency of 2MHz at different temperatures ranging from 298.15K to 313.15K at 5K intervals. The temperature was controlled by a thermostat accurate to within ±0.05K. The precision of the ultrasonic velocity measurements was within ± 0.5 ms^{-1}.

Density measurement

The densities of solutions were measured by relative measurement method using a specific gravity bottle (25 mL capacity) as described earlier[7]. At least five observations were taken and the differences in any two readings did not exceed ±0.02%.

Viscosity measurement

Viscosity measurements were made as described earlier8 using an Ostwald viscometer in a water thermostat whose temperature was controlled to ±0.05K and efflux time was determined using a digital stop clock with an accuracy of ±0.01s. An average of three sets of flow times for each solution was taken for the calculation of viscosity. The values of viscosity so obtained were accurate to within ±0.3 × 10^{-3}cp.

Theoretical Aspects

From the experimental values of ultrasonic velocity *(U)*, density *(d)* and viscosity *(η)* the following thermo-acoustical parameters have been calculated[9-14].

Free volume (V_f)

The free volume is the effective volume in which particular molecule of the liquid can move and obey perfect gas laws. According to Eyring and Kincaid, free volume in terms of ultrasonic velocity *(U)* and the viscosity of the liquid *(η)* is given by,

$$V_f = \left(M_{eff} U / K\eta\right)^{3/2} \quad (1)$$

where $M_{eff} = \sum n_i m_i / \sum n_i$ is the effective molecular weight, $K = 4.281 \times 10^9$ is the dimensionless constant independent of temperature and nature of liquid.

Internal pressure (π_i)

The internal pressure is the cohesive force, which is a resultant of force of attraction and repulsion between the molecules. It is also an important parameter to study the thermodynamic properties and gives an idea of the solubility characteristics of liquids. According to Suryanarayan, the internal pressure is obtained by the formula,

$$\pi_i = b' RT\,(K\eta / U)^{1/2} (d^{2/3} / M_{eff}^{7/6}) \quad (2)$$

where $b' = 2$ is the cubic packing factor for all liquids, R is the Universal gas constant= 8.3143 $JK^{-1}mol^{-1}$ and T is the temperature in Kelvin.

Relaxation time (τ)

Relaxation time is the time taken for the excitation energy to appear as translational energy and it depends on temperature and on impurities. The relaxation time *(τ)* can be calculated from the relation.

$$\tau = 4\eta / 3U^2 d \quad (3)$$

Gibb's free energy change (ΔG)

The relaxation time for a given transition is related to the activation free energy. The variation of τ with temperature can be expressed in the form of Eyring salt process theory $\frac{1}{\tau} = \frac{k_B T}{h} \exp\left(\frac{-\Delta G}{k_B T}\right)$.

or, $$\Delta G = k_B T ln\left(k_B T \tau / h\right) \quad (4)$$

where k_B is the Boltzmann's constant = 1.38 × 10^{-23} JK^{-1} $molecule^{-1}$ and h is Planck's constant = 6.626 × 10^{-34} Js.

Ultrasonic attenuation (a/f^2)

Ultrasonic attenuation can be computed from ultrasonic velocity by the following relation

$$a / f^2 = 4\pi^2 \tau / 2U \quad (5)$$

where f is the frequency of ultrasonic wave (= 2MHz).

van der Waals constant (b)

The van der Walls constant is also known as co-volume in the van der Walls equation and is calculated from the relation,

$$b = \frac{M_{eff}}{d}\left[1-\left(\frac{RT}{M_{eff}U^2}\right)\left\{\left(1+\frac{M_{eff}U^2}{3RT}\right)^{1/2}-1\right\}\right] \qquad (6)$$

Results and discussion

As observed previously[5], the values of ultrasonic velocity *(U)* increase with the increase of ethanol content in water as well as the concentrations of electrolytes (Metal chlorides) in various solvent systems (5, 10 and 15 wt% of ethanol + water). Ultrasonic velocity tends to increase due to increase in molecular mass of electrolytes and it also increases with increase in temperature in all the solvent systems. With increase in temperature, there occurs a structural arrangement leading to a comparatively more order state resulting in increase in velocity. It also suggests that disruption of water structure is enhanced with the addition of ethanol and electrolyte. This is well agreeing with the earlier studies in various mixed solvent systems[12, 15]. The density *(d)* and viscosity *(η)* of the electrolytes (magnesium chloride and zinc chloride) in aqueous ethanol increase with the increase in concentration of solution due to association occurs between solute and solvent molecules[16] and decrease with rise of temperature due to thermal energy of the system which diminishes the intermolecular forces[17]. Typical plots of ultrasonic velocity *(U)* versus concentration *(c)* are shown in Fig. 1(a)-(b).

The free volume (V_f) is the effective volume accessible to the centre of a molecule in a liquid. The structure of a liquid is determined by strong repulsive forces in the liquid with the relatively weak attractive forces providing the internal pressure which held the liquid molecules

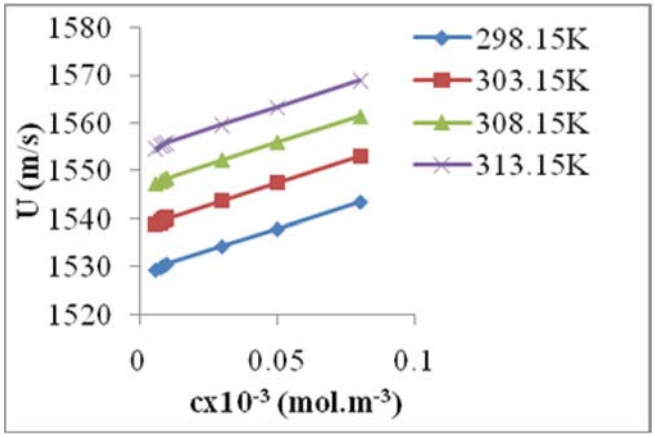

Fig. 1. (a) Plot of *U* versus *c* for $MgCl_2$ in 5 wt% ethanol + water at different temperatures

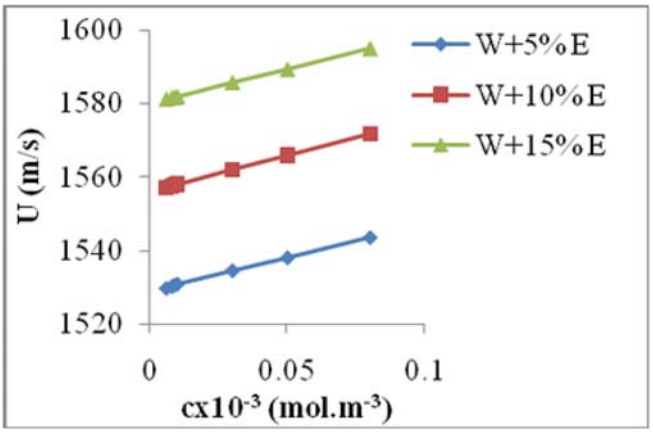

Fig. 1. (b) Plot of *U* versus *c* for $MgCl_2$ in different aqueous ethanol solution at 298.15K

together. The free volume seems to be conditional by repulsive forces whereas the internal pressure is more sensitive to attractive forces. These two factors together uniquely determine the entropy of the system. Thus, the internal pressure, free volume and temperature seem to be the thermodynamic variables that describe the liquid system of fixed composition[12]. From Table 1, it is observed that the free volume (V_f) decreases with increase in concentration and increases with temperature for all solvent systems. Further, it decreases with increase in ethanol content in water. Internal pressure (π_i) changes in a manner opposite to that of free volume at all temperatures. The decrease of V_f (or increase of π_i) indicates the formation of hard and/or tight solvation layer around the ion due to more solute-solvent interaction[18]. With increase in temperature, thermal energy of the molecules increases, hence available free volume (V_f) increases (or π_i decreases). As observed the free volume (V_f) follow the order: $ZnCl_2 > MgCl_2$. The available free volume (V_f) in aqueous ethanol solutions are less as compared to water[5] indicates the presence of hydrogen bonding and suggests more solvent-solvent interactions. Typical plots of V_f versus *c* are shown in Fig. 2(a)-(b).

As observed from Table 2, the relaxation time (τ) increases with increase in ethanol content in water as well as concentration of electrolytes in all aqueous ethanol systems at all temperatures suggesting the rearrangement of molecules due to co-operation process and reinforcement of H-bonds[19,20]. With rise in temperature, H-bonds become weak due to thermal vibration resulting in structure breaking effect that predominates over H-bond formation, and hence, τ

Table 1 – Values of π_i (Nm^{-2}), V_f ($m^3.mol^{-1}$) and b ($m^3.mol^{-1}$) of electrolytes in aqueous ethanol systems at different temperatures

$c \times 10^{-3}$ ($mol.m^{-3}$)	$\pi_i \times 10^{-6}$				$V_f \times 10^7$				$b \times 10^6$			
	Temperature(K)											
	298.15	303.15	308.15	313.15	298.15	303.15	308.15	313.15	298.15	303.15	308.15	313.15
Magnesium chloride + 5 wt % ethanol + water												
0.006	2694.7	2573.2	2463.8	2358.1	0.162	0.195	0.232	0.277	17.836	17.863	17.891	17.921
0.009	2738.6	2646.3	2513.0	2401.6	0.154	0.179	0.219	0.262	17.830	17.857	17.885	17.915
0.030	2781.4	2665.8	2537.3	2423.8	0.147	0.175	0.213	0.255	17.831	17.855	17.883	17.914
0.080	2807.2	2686.2	2578.5	2456.3	0.143	0.171	0.203	0.245	17.836	17.860	17.887	17.919
Magnesium chloride + 10 wt % ethanol + water												
0.006	2748.7	2588.1	2457.5	2357.9	0.131	0.164	0.200	0.237	19.343	19.372	19.402	19.435
0.009	2765.1	2606.1	2478.1	2375.2	0.128	0.160	0.195	0.232	19.341	19.370	19.400	19.433
0.030	2778.3	2637.5	2508.1	2397.9	0.126	0.155	0.188	0.225	19.342	19.370	19.401	19.434
0.080	2818.4	2661.7	2628.3	2518.6	0.121	0.151	0.164	0.195	19.350	19.379	19.409	19.442
Magnesium chloride + 15 wt % ethanol + water												
0.006	2720.8	2608.9	2497.8	2350.5	0.116	0.138	0.165	0.207	20.868	20.897	20.927	20.960
0.009	2738.6	2628.9	2508.4	2369.6	0.114	0.135	0.163	0.202	20.860	20.888	20.919	20.952
0.030	2766.3	2644.9	2515.7	2388.6	0.111	0.133	0.162	0.197	20.856	20.885	20.915	20.949
0.080	2776.4	2656.2	2524.8	2396.9	0.110	0.131	0.160	0.195	20.854	20.883	20.913	20.947
Zinc chloride + 5 wt % ethanol + water												
0.006	2678.0	2539.7	2410.5	2331.5	0.164	0.202	0.247	0.285	17.881	17.909	17.945	17.984
0.009	2694.7	2555.2	2431.6	2347.5	0.161	0.198	0.240	0.279	17.877	17.905	17.941	17.982
0.030	2703.8	2567.0	2449.7	2360.0	0.159	0.195	0.235	0.274	17.888	17.920	17.956	17.995
0.080	2721.5	2596.5	2472.0	2378.0	0.156	0.189	0.229	0.268	17.895	17.923	17.958	17.998
Zinc chloride + 10 wt % ethanol + water												
0.006	2674.2	2532.7	2428.7	2305.4	0.141	0.174	0.206	0.252	19.380	19.413	19.450	19.491
0.009	2687.5	2541.6	2439.5	2316.0	0.139	0.172	0.204	0.249	19.381	19.415	19.452	19.492
0.030	2697.5	2549.9	2446.9	2322.1	0.138	0.170	0.202	0.247	19.387	19.424	19.461	19.502
0.080	2706.5	2557.7	2457.0	2337.7	0.136	0.169	0.199	0.242	19.396	19.434	19.470	19.511
Zinc chloride + 15 wt % ethanol + water												
0.006	2654.1	2505.5	2395.2	2248.2	0.125	0.155	0.186	0.234	20.918	20.956	20.998	21.046
0.009	2669.5	2516.6	2407.5	2266.1	0.123	0.153	0.183	0.229	20.908	20.946	20.984	21.031
0.030	2679.4	2528.9	2419.5	2277.1	0.122	0.151	0.181	0.226	20.902	20.944	20.982	21.024
0.080	2701.6	2561.9	2453.7	2309.4	0.118	0.145	0.173	0.217	20.919	20.962	21.000	21.042

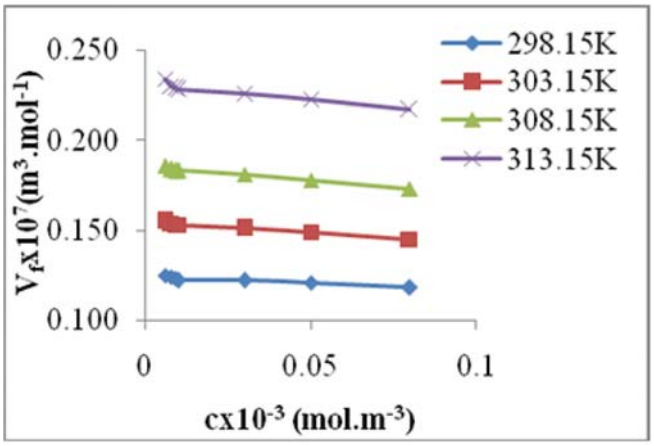

Fig. 2. (a) Plot of V_f versus c for $ZnCl_2$ in 15 wt% ethanol + water at different temperatures

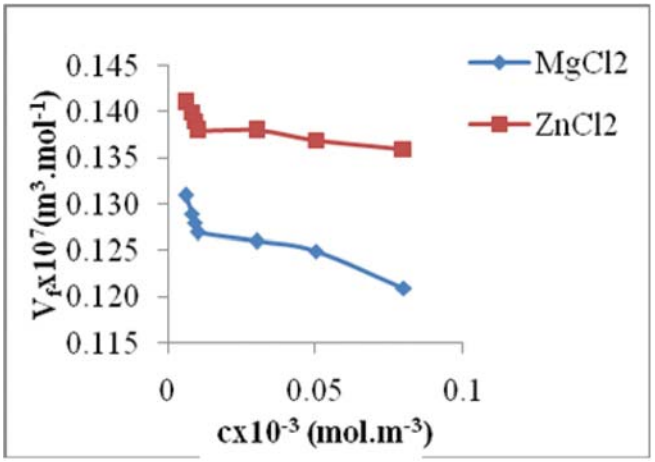

Fig. 2. (b) Plot of V_f versus c for different electrolytes in 10 wt% ethanol + water at 298.15K

Table 2 – Values of τ (s), ΔG (kJ.mol^{-1}) and α/f^2 (Np.m^{-1}) of electrolytes in aqueous ethanol systems at different temperatures.

$c \times 10^{-3}$ (mol.m^{-3})	$\pi \times 10^{13}$				$\Delta G \times 10^{20}$				$\alpha/f^2 \times 10^{15}$			
	Temperature(K)											
	298.15	303.15	308.15	313.15	298.15	303.15	308.15	313.15	298.15	303.15	308.15	313.15
Magnesium chloride + 5 wt % ethanol + water												
0.006	6.245	5.496	4.869	4.318	0.558	0.521	0.485	0.447	8.062	7.051	6.213	5.483
0.009	6.441	5.804	5.059	4.472	0.570	0.543	0.501	0.463	8.310	7.443	6.451	5.676
0.030	6.624	5.871	5.139	4.540	0.582	0.548	0.508	0.469	8.524	7.508	6.536	5.747
0.080	6.705	5.922	5.273	4.633	0.587	0.552	0.519	0.478	8.576	7.529	6.668	5.830
Magnesium chloride + 10 wt % ethanol + water												
0.006	7.655	6.563	5.731	5.116	0.641	0.595	0.554	0.521	9.707	8.288	7.210	6.416
0.009	7.741	6.651	5.823	5.188	0.646	0.600	0.561	0.527	9.813	8.396	7.323	6.504
0.030	7.790	6.790	5.946	5.271	0.649	0.609	0.570	0.534	9.848	8.548	7.457	6.590
0.080	7.966	6.872	6.489	5.779	0.658	0.614	0.607	0.573	10.01	8.599	8.089	7.182
Magnesium chloride + 15 wt % ethanol + water												
0.006	8.756	7.805	6.942	5.973	0.697	0.667	0.635	0.588	10.93	9.729	8.639	7.423
0.009	8.859	7.914	6.991	6.062	0.702	0.673	0.638	0.594	11.06	9.861	8.696	7.530
0.030	9.008	7.983	7.009	6.139	0.708	0.677	0.639	0.600	11.22	9.922	8.696	7.606
0.080	9.009	7.994	7.008	6.137	0.708	0.677	0.639	0.599	11.15	9.876	8.645	7.560
Zinc chloride + 5 wt % ethanol + water												
0.006	6.187	5.369	4.677	4.238	0.554	0.511	0.467	0.439	7.967	6.870	5.949	5.362
0.009	6.257	5.429	4.753	4.292	0.558	0.515	0.474	0.445	8.053	6.943	6.043	5.428
0.030	6.285	5.469	4.816	4.330	0.560	0.519	0.480	0.449	8.064	6.973	6.105	5.460
0.080	6.317	5.549	4.864	4.360	0.562	0.525	0.484	0.452	8.047	7.023	6.120	5.458
Zinc chloride + 10 wt % ethanol + water												
0.006	7.255	6.293	5.605	4.901	0.619	0.577	0.544	0.502	9.174	7.920	7.025	6.121
0.009	7.324	6.335	5.653	4.944	0.623	0.580	0.548	0.506	9.257	7.969	7.083	6.172
0.030	7.358	6.361	5.674	4.958	0.625	0.582	0.550	0.507	9.273	7.980	7.088	6.172
0.080	7.353	6.354	5.680	4.990	0.625	0.581	0.550	0.510	9.203	7.915	7.046	6.170
Zinc chloride + 15 wt % ethanol + water												
0.006	8.350	7.215	6.401	5.485	0.677	0.634	0.601	0.551	10.40	8.958	7.930	6.782
0.009	8.433	7.266	6.454	5.560	0.681	0.637	0.604	0.557	10.50	9.018	7.992	6.872
0.030	8.459	7.309	6.493	5.590	0.683	0.640	0.607	0.559	10.49	9.043	8.015	6.888
0.080	8.545	7.454	6.635	5.713	0.687	0.648	0.616	0.569	10.53	9.159	8.134	6.991

decreases with temperature for the studied electrolytes in all aqueous ethanol systems[21].

Gibb's free energy change *(ΔG)* increases slowly with increase in concentration of electrolytes at all temperatures in all solvent systems. This suggests shorter time for rearrangement of molecules. With rise in temperature, *ΔG* decreases due to increase in kinetic energy of the molecules by thermal energy and takes longer time for rearrangement of molecules for a given concentration in all the solvent systems[22]. Also *ΔG* increases with increase in ethanol content in water suggests the closer approach of unlike molecules due to H-bond formation. Typical plots of *ΔG* versus *c* are shown in Fig. 3(a)-(b).

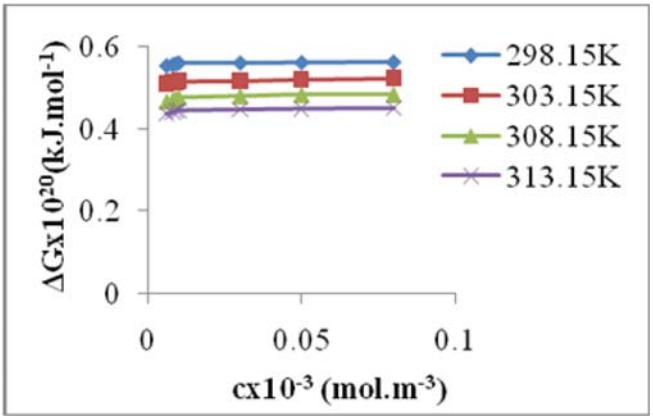

Fig. 3. (a) Plot of *ΔG* versus *c* for $ZnCl_2$ in 5 wt% ethanol + water at different temperatures

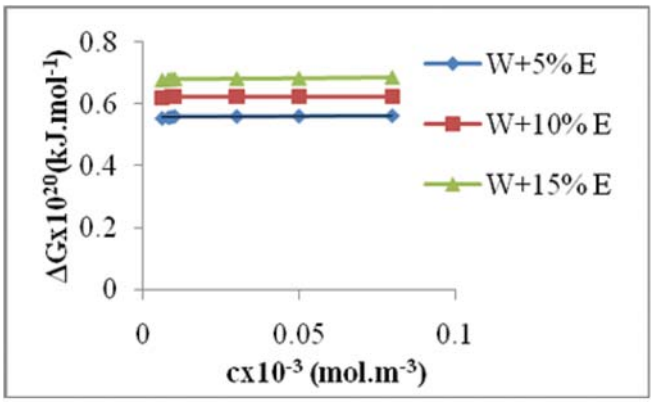

Fig. 3. (b) Plot of ΔG versus *c* for $ZnCl_2$ in different aqueous ethanol solution at 298.15K

Ultrasonic attenuation (α/f^2) is a measure of spatial rate of decrease in the intensity level of the ultrasonic wave, and attenuation co-efficient (α) depends upon the external conditions like temperature, pressure and frequency of the measurement. Ultrasonic attenuation increases with increase in ethanol content in water and concentration of electrolytes (except in few cases) may be due to compact packing of the medium, but it decreases with rise in temperature for the electrolytes in all the solvent systems as given in Table 2.

As observed, van der Walls constant (b) is increasing almost linearly with concentrations as well as with rise in temperature which indicates the binding forces between the solute and solvent in the solution becomes stronger and there exist a strong molecular interaction and binding forces between the solute and solvent molecules. Further, it increases with increase in ethanol content in water. Typical plots of *b* versus *c* are shown in Fig. 4.

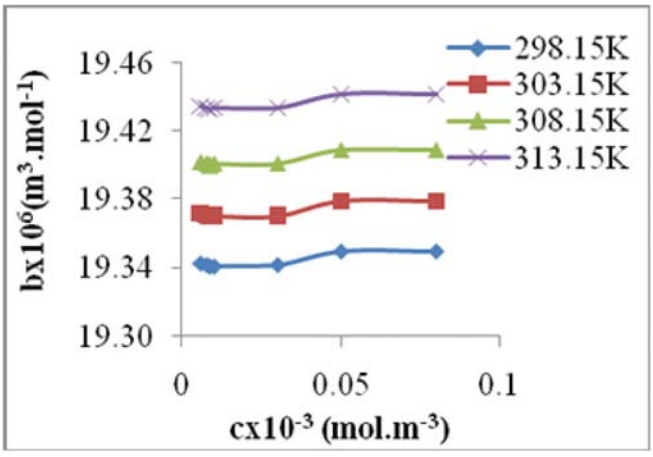

Fig. 4. Plot of b versus *c* for $MgCl_2$ in 10wt% ethanol + water at different temperatures

Conclusions

Ultrasonic technique is a powerful tool for characterising the physical properties and existence of molecular interaction in the mixture. The results of the present investigation reveal that solute-solvent and solvent-solvent interactions play a vital role for explaining the different thermo-acoustical parameters of strong electrolytes in different aqueous ethanol systems at four different temperatures 298.15K, 303.15K, 308.15K and 313.15K. These interactions result in attractive forces which promote the structure forming tendency. It is also noticed that the strength of molecular interaction weakens with rise of temperature which may be due to weak intermolecular forces and thermal energy of the system. The decrease of free volume (or increase of π_i) with increase in concentration and ethanol content in water indicates the formation of hard and/or tight solvation layer around the ion making the systems less compressible.

Acknowledgements

The authors thankfully acknowledge the support and facilities provided by DRIEMS, Tangi, Cuttack, India to carry out the research work in the institution.

References

1 **Nithiyanantham S.** and **Palaniappan L.**, Acoustical studies on some disaccharides (sucrose, lactose, maltose) in aqueous media at room temperature, *Metals Mate. Proces.*, **20** (2008) 203-208.

2 **Palaniappan L.** and **Karthikeyan V.**, Study of acoustical parameters of binary liquid mixtures at 298K *Ind. J. Phys.*, **79** (2005) 155.

3 **Ravichandran S.** and **Ramanathan K.**, Ultrasonic investigations of $MnSO_4$, $NiSO_4$ and $CuSO_4$ aqueous in polyvinyl alcohol solution at 303K, *Rasayan J. Chem.*, **3** (2010) 375-384.

4 **Kannappan V.** and **Jaya Santhi R.**, Ultrasonic studies of isomeric butyl alcohol in aqueous solutions, *Indian J. Pure & Appl. Phys.*, **43** (2005) 167-171.

5 **Swain B., Mishra R.N.** and **Dash U.N.**, Ultrasonic studies on molecular interactions in strong electrolytes-Metal chlorides in aqueous medium at different temperatures and 2 MHz frequency, *Int. J. Adv. Res.*, **4** (2016) 427-439.

6 **Robinson R.A.** and **Stokes R.H.**, Electrolyte Solutions, Butterworth's Scientific Publication, London, (1955) 30.

7 **Swain B., Mishra R.N.** and **Dash U.N.**, Volumetric study of strong electrolytes-metal chlorides and metal sulphates in aqueous medium at different temperatures, *J. Chem. Pharm. Res.*, **7** (2015) 140-144.

8 **Swain B., Mishra R.N.** and **Dash U.N.**, Viscometric and thermodynamic studies on strong electrolytes - Metal chlorides and metal sulphates in aqueous medium at different temperatures, *Int. J. Chem. Phys. Sci.*, **4** (2015) 66-76.

9 **Eyring H.** and **Kincaid J.F.**, Free volume and free angle ratio of molecules in liquid, *J. Chem. Phys.*, **6** (1938) 620.

10 **Suryanarayan C.V.**, Internal pressure and free volume-The key parameters in characterizing liquids and electrolyte solutions, *J. Acoust. Soc. Ind.*, **7** (1979) 131.

11 **Talukdar M., Moharatha D., Roy G.S.** and **Dash U.N.**, Acoustic and ultrasonic studies of alkali metals and ammonium halides in chitosan solutions at four different temperatures, *Indian J. Pure & Appl. Phys.*, **51** (2013) 202-206.

12 **Das S.** and **Dash U.N.**, Evaluation of thermo-acoustic and non-linearity parameter (B/A) of Glycine, -alanine, ?-alanine and phenyl alanine in D-fructose solutions at 298.15K, *Int. J. Pharm. Sci. Rev. Res.*, **21** (2013) 212220.

13 **Palani R.** and **Balakrishnan S.**, Acoustical properties of ternary mixtures of 1-alkanols in di-isopropyl ether and 2, 2, 2-trifluoroethanol mixed solvent, *Indian J. Pure & Appl. Phys.*, **48** (2010) 644-650.

14 **Ali A.** and **Nain A.K.,** Study of molecular interactions in non aqueous binary liquid mixtures through ultrasonic measurements, *J. Pure Appl. Ultrason.*, **22** (2000) 10.

15 **Dash U.N.** and **Sahu R.**, Ultrasonic studies on ammonium salts in aqueous ethereal solvent systems, *Acoustics Lett.*, **17** (1994) 157-164.

16 **Malasane P.R.**, Study of Interactions of Tryptophan through Acoustic and Thermodynamic Properties, *Res. J. Chem. Sci.*, **3** (2013) 73-77.

17 **Roy M.N., Bhattacharjee A.** and **Chanda R.**, Molecular interactions of selected amino acids in aqueous resorcinol solutions: volumetric, viscometric and acoustic studies, *Indian J. Sci. Technol.*, **2** (2009) 63-72.

18 **Syal V.K., Chauhan S.** and **Gautam R.**, Ultrasonic velocity measurements of carbohydrates in binary mixtures of DMSO + H_2O at 25°C, *Ultrasonics*, **36** (1998) 619-623.

19 **Mehra R.** and **Vats S.**, Viscometric, volumetric and thermoacoustic behaviour of amino acids in Urea (aq), *Int. J. Adv. Res.*, **2** (2014) 141-157.

20 **Ali A., Hyder S.** and **Nain A.K.**, Intermolecular interactions in ternary liquid mixtures by ultrasonic velocity measure-ments, *Indian J. Phys. B*, **74** (2000) 63-67.

21 **Wadekar M.P.**, Thermo acoustical molecular interaction study of azomethine and its Fe(III) metal complex using ultrasonic technique, *J. Chem. Pharm. Res.*, **5** (2013) 37-41.

22 **Fort R.J.** and **Moore W.R.**, Adiabatic compressibilities of binary liquid mixtures, *Trans. Faraday Soc.*, **61** (1965) 102-111.

J. Pure Appl. Ultrason. 40 (2018) pp. 80-83

Study of ultrasonic velocity in DBP-polar liquid mixtures

N. Mohanty and R. Paikaray*

Department of Physics, Ravenshaw University, Cuttack-753003, India
*E-mail: r_paikaray@rediffmail.com

Ultrasonic velocity of binary mixture of Di-n-butyl phthalate (DBP) with polar liquid aniline is measured experimentally at different frequencies (1MHz, 3MHz, 5MHz and 7MHz) and at constant temperature 308K. Using theoretical relations such as Nomoto's relation (NR), Free length theory (FLT), and ideal mixing relation (IMR), Junjie's relation(JM), and Schaaffs collision factor theory(CFT) ultrasonic velocity (U) is evaluated at constant temperature 308K and at frequencies 1MHz, 3MHz, 5MHz and 7MHz for the binary mixture of DBP with aniline. The percentage of deviation of experimental values from theoretical values and average absolute percentage of deviation (AAPD) are calculated. The relative applicability and merits of these theories were checked and discussed.

Keywords: Binary mixture, ultrasonic velocity, frequency.

Introduction

Investigation into the changes of properties of the mixture and their degree of deviation from ideality has been found to be a qualitative and quantitative way to get the information about the molecular structure and intermolecular forces in liquid mixture. The study of the properties of liquid mixtures consisting of polar with polar components find applications in industrial, technological process[1-4] and other related areas. Ultrasonic investigation of liquid mixture basing on polarity is of considerable importance in understanding intermolecular interaction between component molecules and gaining insight into structure and bonding of component molecules and other molecular processes[5-8]. The properties of liquid mixture basically depend on its local structure, packing density, volume and composition. These changes in composition changes the acoustic, thermodynamic properties of the liquid mixture[7]. The validity of these formulations for ultrasonic response of the above said binary mixture has been examined and the results are analyzed to show the feasibility of the theoretical models which envisage the increasing deviation with increasing non ideality in the mixture.

Materials and Method

The mixtures of DBP with aniline were prepared by mixing the calculated values. The mass measurement was made using an electronic balance. The accuracy of density measurement is 5%. The velocity of sound was measured by using interferometer with frequencies 1 MHz, 3 MHz, 5 MHz and 7 MHz at constant temperature 308 K which was controlled by using temperature bath with an accuracy of 0.01 K. Theoretical formulae of ultrasonic velocity in binary mixture are computed using empirical relations basing on different models[9-13].

Results and Discussion

DBP being a polar liquid interacts with above said polar and non-polar liquids and all these components have extensive applications in various fields. Pure aniline being polar there is dipole-dipole as well as dispersive interactions between the molecules of aniline and by adding DBP a second polar it disrupts the dipolar interaction of aniline but as both are polar, the dipole-dipole interaction between unlike polar molecules is most likely to occur[13]. However, the behavior of the liquid mixture depends on the relative strength of dispersive forces of molecules and chemical dipole-

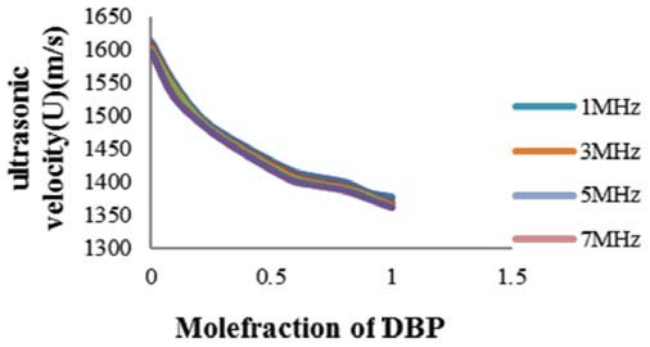

Fig. 1. Ultrasonic Velocity vs. Mole fractions of DBP

dipole interaction force[14]. Experimental measured values of ultrasonic velocity at 308K and at different frequencies (1 MHz, 3 MHz, 5 MHz and 7 MHz) for different mole fractions are given Fig. 1.

Ultrasonic velocity decreases at a higher rate in aniline rich region (up to 0.57 molefraction of DBP). It is also observed that ultrasonic velocity decreases with the increase in frequency. A higher density of component molecules is a reflection of higher intermolecular interaction. Hence, in this binary mixture a high degree of intermolecular interaction is expected. The decreasing trend of ultrasonic velocity indicates weak dipole-dipole interaction of unlike molecules and it may be due to the structural changes between the unlike molecules[14]. With increase in frequency, the interaction becomes weaker resulting decrease in velocity.

Theoretical evaluation of sound velocity in the binary mixture of DBP and aniline at said frequencies at 308K and its comparisons with experimental values reflecting the molecular interaction in liquid which is useful to build comprehensive theoretical model for liquid mixture is carried out. Figures 2, 3, 4 and 5 represent the experimental and computed theoretical ultrasonic velocities.

Figure 2 indicates that at 1MHz frequency JM and NR show very good match with experimental values and closely followed by free length theory. In this case CFT gives a good agreement with the experimental velocity. IMR shows higher deviation as in other binary mixtures of this research work, but the deviation is much less in comparison to others and it is around 4.5%. The average absolute percentage deviation is small in the systems having less interaction. The AAPD value of this system at 1MHz frequency indicates weak interaction between DBP and aniline.

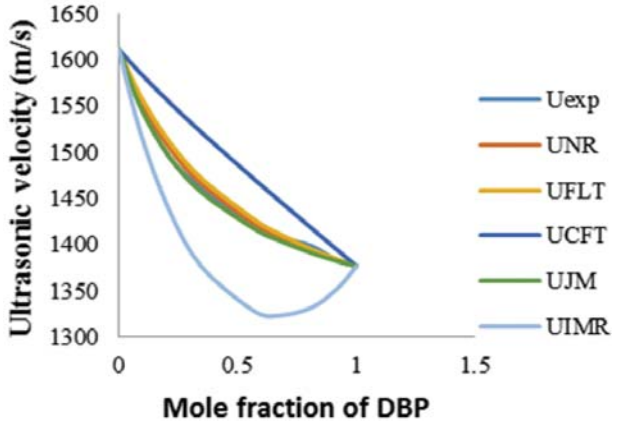

Fig. 2. Variation of experimental (Uexp) and theoretical values of Ultrasonic velocity with Mole fraction of DBP (1MHz)

Figure 3 reveals that binary mixture of DBP and aniline at 3 MHz and 308 K, NR, JM and FLT have good agreement with experimental values. CFT also well fits reasonably with the experimental value since their AAPD value is less than 3%. IMR shows a deviation of 4.6% as in case of 1MHz frequency.

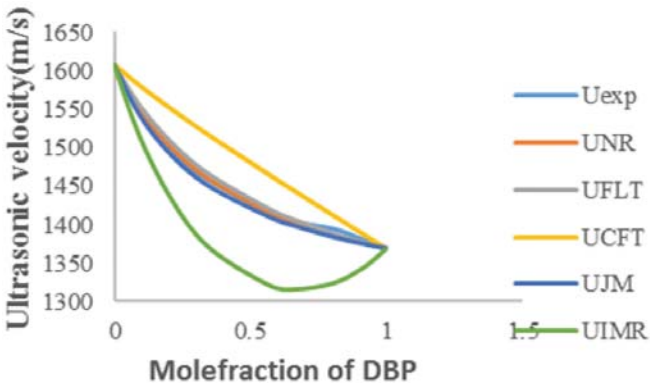

Fig. 3. Variation of experimental (Uexp) and theoretical values of Ultrasonic velocity with Mole fraction of DBP (3MHz)

At 5 MHz frequency it is observed from Fig. 4 that NR shows slight deviations (0.25%) followed by FLT and then JM. CFT also show small deviations from experimental values (AAPD < 3%) whereas higher deviations is observed in IMR (AAPD < 5%).

Figure 5 of the binary mixture DBP and aniline at 7 MHz frequency reveals that there is a good agreement between experimental and theoretical value calculated by NR, JM and FLT (AAPD<0.51%). CFT shows moderate deviations (AAPD<3%) while higher deviation is observed in case of ideal mixing relation.

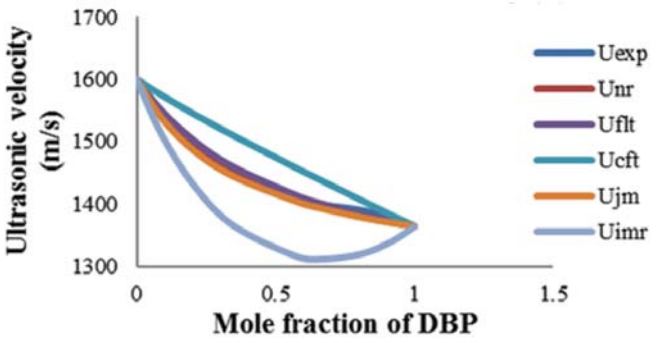

Fig. 4. Variation of experimental (Uexp) and theoretical values of Ultrasonic velocity with Mole fraction of DBP at (5MHz)

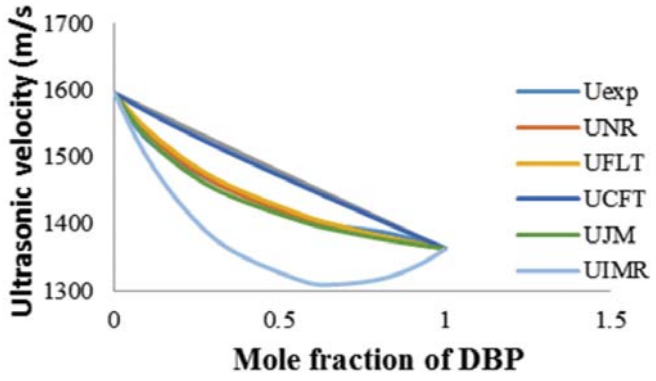

Fig. 5. Variation of experimental (Uexp) and theoretical values of Ultrasonic velocity with Mole fraction of DBP (7MHz)

It is observed that sound velocity for DBP and aniline mixture for different frequencies has not unique order of applicability of theoretical evaluation. In all the said four frequencies at 308 K, Nomoto's relations, Junjie's method and free length theory are most suitable models for evaluation of velocity. The order of applicability of the models in this system for all the said frequencies is:

$U_{JM} > U_{NR} > U_{FLT} > U_{CFT} > U_{IMR}$ for 1 MHz

$U_{NR} > U_{JM} > U_{FLT} > U_{CFT} > U_{IMR}$ for 3 MHz

$U_{NR} > U_{FLT} > U_{JM} > U_{CFT} > U_{IMR}$ for 5 MHz

$U_{NR} > U_{JM} > U_{FLT} > U_{CFT} > U_{IMR}$ for 7 MHz

The interaction parameter found to be negative for all said frequencies indicating weak interaction between component molecules in the binary mixture of DBP and aniline. All the models have good predictive abilities (maximum AAPD< 5%) indicating weak interaction which is supposed to exist in this liquid mixture.

Conclusions

DBP with polar liquids such as aniline shows weak interactions. According to the strength of interaction, deviations of theoretical values from experimental values are observed. The deviations are due to approximations and limitations taken by the researchers in developing the theoretical models/formulations. Various types of forces such as dispersion forces, charge transfer, hydrogen bonding, dipole-dipole and dipole-induced dipole exist inside the liquid mixture due to interaction of molecules which are also responsible for the deviations. The orders of applicability of the theoretical models are different from system to system and for different frequencies. However ideal mixing relation (IMR) shows the higher deviations. On increasing the frequency, ultrasonic velocity decreases which may be due to the increase in vibrational energy which activates the molecules and there may be increase in rate of association of unlike molecules. It is also observed in all four frequencies for all binary mixtures that the deviations in ultrasonic velocities decrease with increase in frequency which may be due to breaking of molecular clusters at higher frequencies.

References

1 **Nath G.** and **Paikaray R.**, Effect of frequency on acoustic parameters in a binary mixture of polar liquids, *Ind. J.Phys.* **83** (2009), 1567-1574.

2 **Paikaray R.** and **Mohanty N.**, Ultrasonic investigation of molecular interactions in a binary mixture of DBP with Benzene at different frequencies, *J. Acoust. Soc. Ind.* **37** (2010), 70-73.

3 **Vysyaraju S. Diwakar P.P.** and **Samatha K.**, Mesurement of ultrasonic velocity in binary liquid mixture of N,N-dimethyl actetamide(NNDA)+diethyl-amine(DEA), *IJIRSET*, **5**(11) (2016), 18972-18978.

4 **Nath G., Sahu S.** and **Paikaray R.**, Acoustical investigation of molecular interaction in binary mixture of acetone and xylene (mixed isomers) at different frequencies, *J. Acoust. Soc. Ind.* **35** (2008), 115-120.

5 **Resa P., Elvira L., Montero de Espinosa F.** and **Gómez-Ullate Y.**, Ultrasonic velocity in water-ethanol-sucrose mixtures during alcoholic fermentation, *Ultrasonics*, **43**(4) (2005), 247-252.

6 **Petak A.** and **Dolcek A.**, Excess molar volumes of binary liquid mixtures of cyclohexane - carbon tetrachloride and

toluene - benzene at various temperatures, *Acta Chem. Slov.* **45** (1998), 153-160.

7 **Sathyanarayana B., Savitha T., Jyostna** and **Satyanarayana N.**, Acoustic studies of binary mixtures of N-methylacetamide with some chloroethanes and chloroethenes at 308.15 K, *Indian J Pure Appl. Phys.* **44** (2006), 587-591.

8 **Zatale D.A., Chaware A.R.** and **Zatale K.D.**, Study and analysis of thermoacoustic parameters of petrochemical product and its mixtures at different temperatures from 298.15K to 318.15K, *Arch. Phys. Res.*, **2**(1) (2011), 202-207.

9 **Rama Rao G.V., Sarma A.V. , Siva J. Krishna R.** and **Ramababu C.**, Theoretical evaluation of ultrasonic velocities in binary liquid mixtures of o-chlorophenol at different temperatures, *Indian J. Pure Appl. Phys.*, **43**(5) (2005), 355-358.

10 **Pandiyan V., Oswal S.L., Malek N.I.** and **Vasantharani P.**, Thermodynamic and acoustic properties of binary mixtures of ethers. V. Diisopropyl ether or oxolane with 2- or 3-chloroanilines at 303.15, 313.15 and 323.15K, *Thermochim. Acta,* **524** (2011), 140-150.

11 **Mohanty N.** and **Paikaray R.**, Theoretical evaluation of ultrasonic velocity of binary mixture of Di-n-Butyl(DBP) with phenol, *Open J. Phys.* **19**(1) (2012), 117-120.

12 **Mohanty N.** and **Paikaray R.**, Evaluation of Thermodynamical Acoustic Parameters of Binary mixture of DBP with Toluene at 308 K and at Different Frequencies, *Res. J. Chem. Sci.,* **3**(5) (2013), 71-82.

13 **Bhatnagar D., Joshi D., Gupta R., Kumar Y., Kumar A.** and **Jain C.L.**, Studies on Thermo acoustic Parameters in binary liquid mixtures of MIBK with 1-Propanol, 1-Butanol and 1-Pentanol at 303.15K-A new approach by Direct Measurement of Acoustic Impedance, *Res. J. Chem. Sci.,* **1**(5) (2011), 6-13.

14 **Rama Rao G.V., Sandhya Sri P.B., Sarma A.V.** and **Rambabu C.**, Comparative study of theoretical ultrasonic velocities of binary mixtures of methanol and pyridine at different temperatures, *Indian J. Pure Appl. Phys.*, **45**(2) (2007), 143-150.

J. Pure Appl. Ultrason. 40 (2018) pp. 84-87

Ultrasonic attenuation in thorium monopnictides

Amit Kumar[1,*], Devraj Singh[2] and R.K. Thakur[1]

[1]Amity School of Applied Sciences, Amity University Haryana, Manesar-122413, India
[2]Amity Institute of Applied Sciences, Amity University, Sector-125, Noida-201313, India
*E-mail: amitrana1711@gmail.com

The ultrasonic attenuation due to phonon-phonon interaction have been computed along <100>, <110> and <111> directions at room temperature. For the evaluation of attenuation, we have also evaluated higher order elastic constant, ultrasonic velocity and acoustic coupling constant. The Coulomb and Born-Mayer potential has been applied to find out the higher order elastic constants in the temperature range 0-300K. Some mechanical constant were also computed for predicting for futuristic performance of the chosen materials. The behaviour of ultrasonic attenuation has been considered in correlated with other thermo-physical properties of thorium monopnictides.

Keywords: Thorium monopnictides, elastic properties, ultrasonic properties.

Introduction

Ultrasonics are the versatile tools for the study of properties of different types of the materials. Monochalogenides and monopnictides of the lanthanides and actinides play important role for engineering and technological applications. Kholia *et al.*[1] have been investigated the structural phase transition and elastic characteristic at high pressure of thorium pnictides. Kumar *et al.*[2] have been calculated the electronic density of states and dielectric properties for the thorium monopnictides with the help of linear muffin tin orbital process not beyond atomic sphere approximation and investigated result have been compared with the accessible experimental data. The high-pressure structural characteristics of a thorium monopnictides have been investigated by using of the all-electron full potential linear muffin-tin orbital process by Kanchana *et al.*[3]. The structural, electronic and elastic belongings of thorium monopnictides using first principles calculation have been investigated by Amari *et al.*[4]. The phonon dispersion curves, two phonon density of states, variation of specific heat, anhormonic characteristic and high pressure phase transition study of ThSe by the application of three-body force shell model and three-body force rigid ion model have been investigated by Dwiwedi *et al.*[5]. The phase transition pressures and volume drop obtained from improved interaction potential model (IIPM) show a better agreement with the available experimental than theoretical results and also achieved elastic moduli, anisotropy factor, Poisson's ratio, Kleinman parameter, shear and stiffness constants on the basis of the calculated elastic constants of thorium monopnictides (ThX; X = N, P, As and Sb) have been investigated by Kapoor *et al.*[6]. Aynyas *et al.*[7] have investigated the structural and elastic characteristic of thorium monopnictides by applying suitable interionic potential at high pressure of thorium pnictides. Gupta *et al.*[8] have inspected the phase transition, elastic and thermophysical properties of thorium pnictides apply by a modified charge-transfer potential model.

In this present paper, we extend the application of elastic and ultrasonic characteristics of thorium monopnictides at different physical condition like temperature and crystallographic directions to make the materials for their futuristic applications.

Theory

The second and third order elastic constant, which depend on temperature have been calculated by applying Coulomb and Born Mayer potential for thorium monopnictides material. The formula of interionic

potential is given bellow:

$$\varphi(r) = \varphi(C) + \varphi(B) \quad (1)$$

Where φ(C) is represent the long range electrostatic/ Coulomb potential and φ(B) is represent the short range repulsive Born-Mayer potential and the formula of φ(C) and φ(B) are given by

$$\varphi(C) = \pm\frac{e^2}{r_0} \text{ and } \varphi(B) = A \exp.\ \frac{-r_0}{b}$$

Where positive and negative sign show that like and unlike ions, e is electronic charge, r_0 is the nearest neighbour distance, b is the hardness parameter and A is the strength parameter[9]. The SOECs and TOECs of a single crystalline material are given below:

$$C_{IJ} = \frac{\partial^2 U}{\partial e_I \partial e_J}, \qquad I \text{ or } J = 1,...., 6$$
$$C_{IJK} = \frac{\partial^3 U}{\partial e_I \partial e_J \partial e_K}, \quad I, J \text{ or } K = 1,...., 6 \quad (2)$$

The second and third order elastic constants (C_{IJ} and C_{IJK})[10] at particular temperature have been represented by following equations:

$$C_{IJ} = C_{IJ}^0 + C_{IJ}^{Vib} \text{ and } C_{IJK} = C_{IJK}^0 + C_{IJK}^{Vib}$$

Where, superscripts 0 and *Vib* show the elastic constants at zero and at particular temperature respectively. The expressions to compute the elastic constants are given in our previous paper[11]. The expressions to compute bulk modulus *(B)*, shear modulus *(G)*, tetragonal modulus *(Cs)*, Poisson's ratio *(σ)* and Zener anisotropy *(A)* have been given in our previous paper[11].

To establish the theory for ultrasonic attention due to phonon-phonon interaction in the chosen thorium monopnictides, Akhiezer[12] proposed this type of theory for first time in the regime (wT≤1). A simplified version was given by Bömmel and Dransfeld[13]. Better version of this theory was given by Woodruff and Ehrenreich[14]. We have applied the modified form of Mason and Bateman theory[15], which is widely applied for different type of materials. The expression for finding ultrasonic attenuation due to phonon-phonon interaction is given in previous paper[16].

Results and Discussion

The SOECs and TOECs have been found out by using the two essential parameters *i.e.*, the lattice parameter and hardness parameter, we have used the input parameters for ThP (lattice parameter a = 5.83Å, hardness parameter b = 0.311Å) and for ThSb (lattice parameter a = 6.10 Å, hardness parameter b = 0.299 Å). The computed SOECs and TOECs have presented in Table 1. We have compared the value of SOECs with first principle results of Kholia *et al.*[1] and Amari *et al.*[4]. Our values are quite different from the results of Kholia *et al.*[1] and Amari *et al.*[4]. Obviously the adopted method of Kholia *et al.*[1] and Amari *et al.*[4] is recent computation with several parameters. But our approach is very straight forward; each and every term in our approach is justified as we checked our results manually as well as computer program in MATLAB. So we also compared our results with other NaCl-type lutetium monochalcogenides[16] and found the same order and variations of SOECs and TOECs for the chosen ThP and ThSb.

From Table 1, we observed that four elastic constants (*i.e.*, C_{12}, C_{111}, C_{123} and C_{166}) value decrease with increase the temperature and elastic constant (C_{11}, C_{44} and C_{144}) value increase with increase the temperature.

Table 1 – Temperature dependent SOECs and TOECs of thorium monopnictides [in GPa]

	Temp. (K)	C_{11}	C_{12}	C_{44}	C_{111}	C_{112}	C_{123}	C_{144}	C_{166}	C_{456}
ThP	100	45.9	9.6	10.4	-783.1	-38.5	12.8	18.1	-42.0	17.9
	200	47.6	8.3	10.4	-792.2	-35.2	7.7	18.2	-42.1	17.9
	300	49.4	8.0	10.5	-801.9	-31.9	2.5	18.3	-42.3	17.9
	300	79.65	7.46							
	300	80.8	12.6	11.7						
ThSb	100	45.9	9.6	10.4	-783.1	-38.5	12.8	18.1	-42.0	17.9
	200	47.6	8.8	10.4	-792.2	-35.2	7.7	18.2	-42.1	17.9
	300	49.4	8.0	10.5	-801.9	-31.9	2.5	18.3	-42.7	17.9
	300	87.3	14.22							
[	300	83.3	10.2	8.61						

Table 2 – *B, G, Cs, σ, A* and *B/G* of thorium monopnictides at 300K

Material	*B*(GPa)	*G*(GPa)	*Cs*(GPa)	σ	*A*	*B/G*
ThP	21.8	17.3		0.418	0.507	1.26
	129[4]	61.6[4]	2.07	0.21[4]	0.21[4]	2.09[4]
ThSb	21.8	17.3		0.418	0.51	1.26
	92.7[4]	30.4[4]	2.07	0.24[4]	0.08[4]	3.04[4]

Table 3 – *D*, τ_{th} (in ps), $(\alpha/f^2)_L$, $(\alpha/f^2)_{S1}$ and $(\alpha/f^2)_{S2}$ (all (α/f^2) in 10^{-16} Np.s^2/m) along <100>, <110> and <111> direction at 300K

Material	Direction	D_L	D_{s1}	D_{s2}	τ^{th}	$(\alpha/f^2)_L$	$(\alpha/f^2)_{S1}$	$(\alpha/f^2)_{S2}$
ThP	<100>	15.07	0.93	0.93	1.10	2.23	1.38	1.38
	<110>	18.51	0.72	27.26	1.36	4.74	1.32	6.47
	<111>	15.47	18.43	18.43	0.88	2.85	10.20	10.20
ThSb	<100>	10.51	0.65	0.65	1.02	1.22	0.77	0.77
	<110>	13.01	0.52	19.16	1.24	2.64	0.76	3.61
	<111>	10.68	12.78	12.78	0.80	1.70	5.79	5.79

The value of elastic constant (C_{456}) is not change with temperature. Second and third order elastic constants value of ThSb material are highest compared to ThP. So, the mechanical effect of ThSb is better than ThP.

The values of SOECs and TOECs are applied to find out the bulk modulus *(B)*, shear modulus *(G)*, Poisson's ratio *(σ)*, tetragonal moduli *(CS)*, Zener anisotropy factor *(A)* and ratio B/G. These parameters are given bellow in Table 2.

The values of B and G are more difference with exiting results4. The ratio B/G (<1.75) shows brittle nature of thorium monopnictides. This type of behaviour is already found in lutetium monochalcogenides[16]. The Born stability criterion is also fulfilled by of thorium monopnictides. The investigated result of Born criterion $C_S = (C_{11} - C_{12})/2 > 0$, this value represent thorium monopnictides is stable in nature.

The thermal relaxation time (τ_{th}), acoustical coupling constant *(D)* and ultrasonic attenuation $\{(\alpha/f^2)_L, (\alpha/f^2)_{S1}$ *and* $(\alpha/f^2)_{S2}\}$ along <100>, <110> and <111> direction at room temperature are given in Table 3.

From Table 3 we found that the conversion of acoustic energy into thermal energy is measured by the acoustic coupling constant. The value of acoustic coupling constant is similar type as for praseodymium monopnictides[23]. The thermal relaxation times have in picoseconds order which represent ThP and ThSb both have semi-metallic in nature[24]. Thermal relaxation time of ThP is greater than ThSb. The value of thermal relaxation time decreases with increase the molecular weight. The value of ultrasonic attenuation of ThP is greater than ThSb

Conclusion

On the basis of above discussion, we conclude that

- Coulomb and Born-Mayer potential has been utilized successfully to calculate higher order elastic constants for thorium monopnictides.
- Thorium monopnictides materials are mechanical stable as they follow Cauchy's stability criterion.
- The ratio *B/G*<1.75, hence thorium monopnictides material are brittle in nature.
- The thermal relaxation time and ultrasonic attenuation values confirm semimetallic behavior of the materials.

The obtained results can be used for further investigation and further study of thorium monopnictides.

References

1 **Kholia K.** and **Gupta B.R.K.**, Structural phase transition and elastic properties of thorium pnictides at high pressure, *Pramana,* **68** (2007) 649-654.

2 **Kumar S.** and **Auluck S.**, Electronic structure and optical properties of thorium monopnictides, *Bull. Mat. Sc.,* **26** (2003) 165-168.

3 **Kanchana V., Vaitheeswaran G., Svane A., Heathman**

S., Gerwarde L. and **Olsen J.S.**, High-pressure study of binary thorium compounds from first principles theory and comparisons with experiment, *Acta Cryst.* **B70** (2014) 459-468.

4 **Amari S., Méçabih S., Abbar B.** and **Bouhafs B.**, First-principle study of structural, elastic and electronic properties of thorium monopnictides, *J. Nucl. Mat.* **454** (2014) 186-191.

5 **Dwiwedi B.P., Mishra K.K.** and **Upadhyaya K.S.**, Crystal dynamic and structural study of thorium selenide (ThSe): elastic behaviour and pressure effect, *Int. J. Rec. Sc. R.,* **3** (2012) 611-620.

6 **Kapoor S., Yaduvanshi N.** and **Singh S.**, Study of phase transformation and elastic properties of ThX (X = N, P, As and Sb) under high-pressure; *Mol. Phys.*. **114** (2016) 3589-3597.

7 **Aynyas M., Sanyal S.P.** and **Jha P.K.**, Structural phase transition and elastic properties of thorium pnictides at high pressure, *Physica Stat. Solidi (b)* **229** (2002) 1459-1466.

8 **Gupta D.C.** and **Baraiya A.K.**, Thermal and elastic properties of thorium pnictides under high pressure; *Phase Transitions,* **83** (2010) 404-418.

9 **Mori S.** and **Hiki Y.**, Calculation of the third- and fourth-order elastic constants of alkali halide crystals, *J. Phys. Soc. Jpn.,* **45** (1975) 1449-1454.

10 **Leibfried G.** and **Hahn H.**, Zur temperatur abhängigkeitder elastischen konstanten von alkali-halogenidkristallen, *Z. Phys.,* **150** (1958) 497-525.

11 **Singh D., Mishra G., Rajkumar** and **Yadav R.R.**, Temperature dependence of elastic and ultrasonic properties of sodium borohydride, *Commun. Phys.,* **27** (2017) 151-164.

12 **Akhiezer A.**, On the Absorption of sound in solids, *J.Phys. (USSR)* **1** (1939)277-287.

13 **Bömmel H.E.** and **Dransfeld K.**, Excitation and attenuation of hypersonic waves in quartz, *Phys. Rev.,* **117** (1960) 1245-1252.

14 **Woodruff T.O.** and **Ehrenreich H.**, Absorption of sound in insulators, *Phys. Rev.,* **123** (1961) 1553-1559.

15 **Mason W.P.** and **Bateman T.B.**, Relation between Third?order elastic moduli and the thermal attenuation of ultrasonic waves in nonconducting and metallic crystals, *J. Acoust. Soc. Am.* **40** (1966) 852-862.

16 **Kumar A., Singh D., Thakur R.K.** and **Kumar R.**, Mechanical and thermophysical properties lutetium monochalcogenides, an ultrasonic study, *J. Pure Appl. Ultrason.* **39** (2017) 43-48.

17 **Pandey D.K., Singh D.** and **Yadav R.R.**, Ultrasonic wave propagation in IIIrd group nitrides, *Appl. Acoust.,* **68** (2007) 766-777.

18 **Singh D.**, Behaviour of acoustic attenuation in rare-earth chalcogenides, *Mat. Chem. Phys.,* **115** (2009) 65-68.

19 **Singh D., Tripathi S., Pandey D.K., Gupta A.K., Singh D.K.** and **Kumar J.**, Ultrasonic wave propagation in semimetallic single crystals, *Mod. Phys. Lett. B,* **31** (2011) 2377-2390.

J. Pure Appl. Ultrason. 40 (2018) pp. 88-90

Short Communications

Design of ultrasonic resonant air-borne tracking system

N.K. Ingle[1,*], L.S. Patil[1], S.U. Dubey[2] and S.J. Sharma[2]

[1]Dr. Annasaheb G. D. Bendale Mahila Mahavidyalaya, Jalgaon-425 001, India
[2]Department of Electronics, R.T.M. Nagpur University, Nagpur-440 033, India
*E-mail: nitin.ingle@yahoo.co.in

Impedance spectroscopy is the study of measurement of impedance and phase with respect to frequency of electrical components or material under study. In the present work, an electrical impedance analysis of air-borne ultrasonic transducers is carried out with the help of a dedicated impedance analyzer, AD5933, manufactured by analog devices. It is a sweep type of resonant frequency tracking instrument that helps to detect the exact resonant frequency for ST 40 and SR 40 transmitter and receiver air borne transducers, respective. It is observed that impedance analyser, AD5933 is effective in the resonant tracking of air borne ultrasonic transducer.

Keywords: Electrical impedance, DDS, DFT, resonance, impedance calibration

Introduction

Impedance is termed as opposition to the alternating current. An impedance of a two-terminal circuit element is the ratio of the complex representation of a sinusoidal voltage between its terminals to the complex representation of the current flowing through it. In general; it depends upon the frequency of the sinusoidal voltage. An electrical impedance analyzer determines the total complex impedance, the total complex impedance. To understand the behaviour of ultrasonic elements, one must review the basics of simple resistance, reactance (inductive and capacitive), the Q factor and parasitic losses. Some of the common methods of impedance measurements are bridge, resonance, IV and RFIV; and network analysis methods.

Electrical impedance spectroscopy (EIS) of ultrasonic transducers and piezoelectric devices derives from the measurement of the current into and the voltage across the transducer as a function of the frequency of applied sinusoidal voltage. The impedance of the ultrasonic transducer can be estimated by applying a sinusoidal voltage to the in series with a resistor, and measuring the voltage across the resistor and across the transducer. Performing this measurement by sweeping the frequencies of the applied signal provides the impedance phase and magnitude.

In present work, we have designed a resonance tracking system to measure impedance of air borne ultrasonic transducers using AD5933 based impedance converter utilising a frequency sweep technique.

Experimental

Poly (ethylene glycol) butyl ether (PEGBE) - 206, 2-(Methylamino) ethanol (MAE) (98.5%) and 1-butanol (99%) were obtained from Sigma-Aldrich Chemicals Ltd. and no further purification was done. Purity of these compounds has been compared with the literature data and is found to be in good agreement as shown in Table 1. Structure of monomer of PEGBE is shown in Fig. 1.

Results and Discussion

The system is calibrated using a precision resistor substituted for the impedance to be measured and a scaling factor is calculated for subsequent measurements, the 200 kΩ resistor is connected across the RFB. After calibration, 200 kΩ resistor is replaced by an air borne ultrasonic transducer and the impedance data is retrieved.

Figure 2 shows the impedance of 40 kHz ultrasonic transducer showing the impedance for resonance and

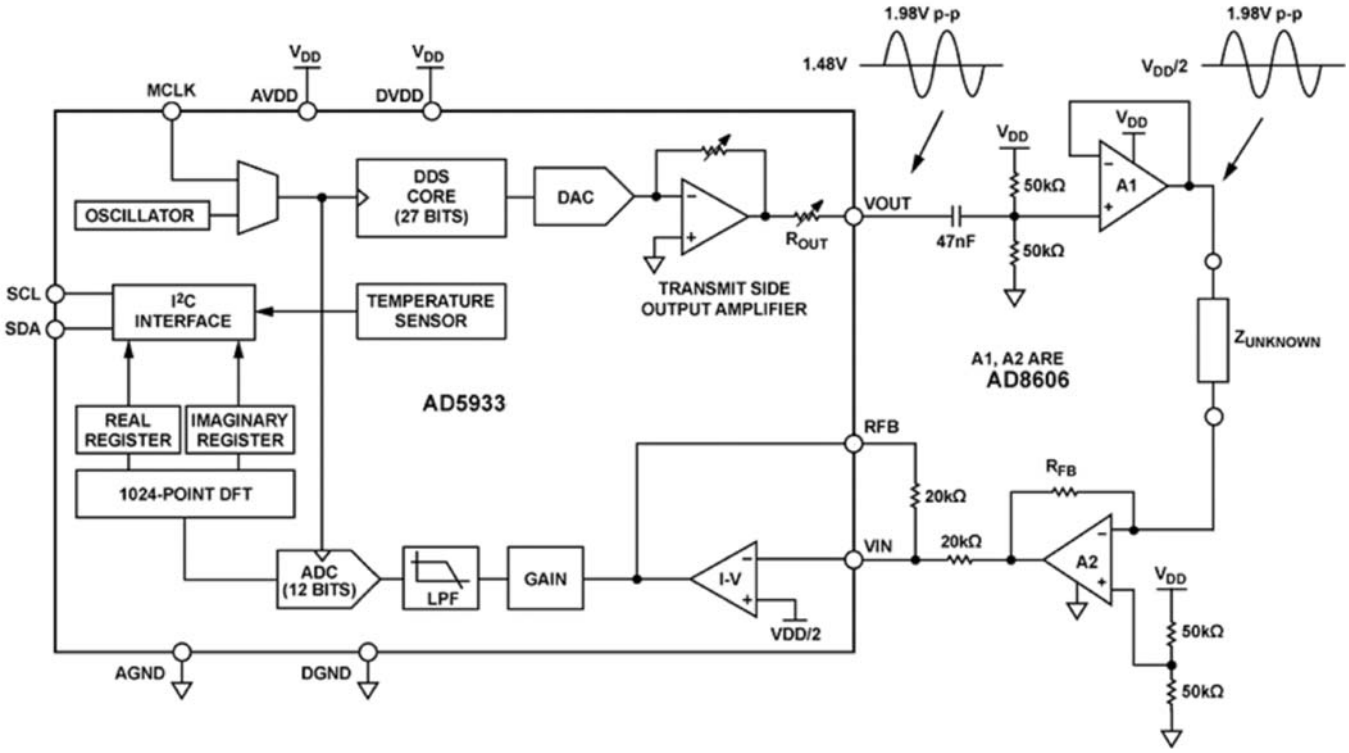

Fig. 1 AD5933 Impedance Convertor Block Diagram

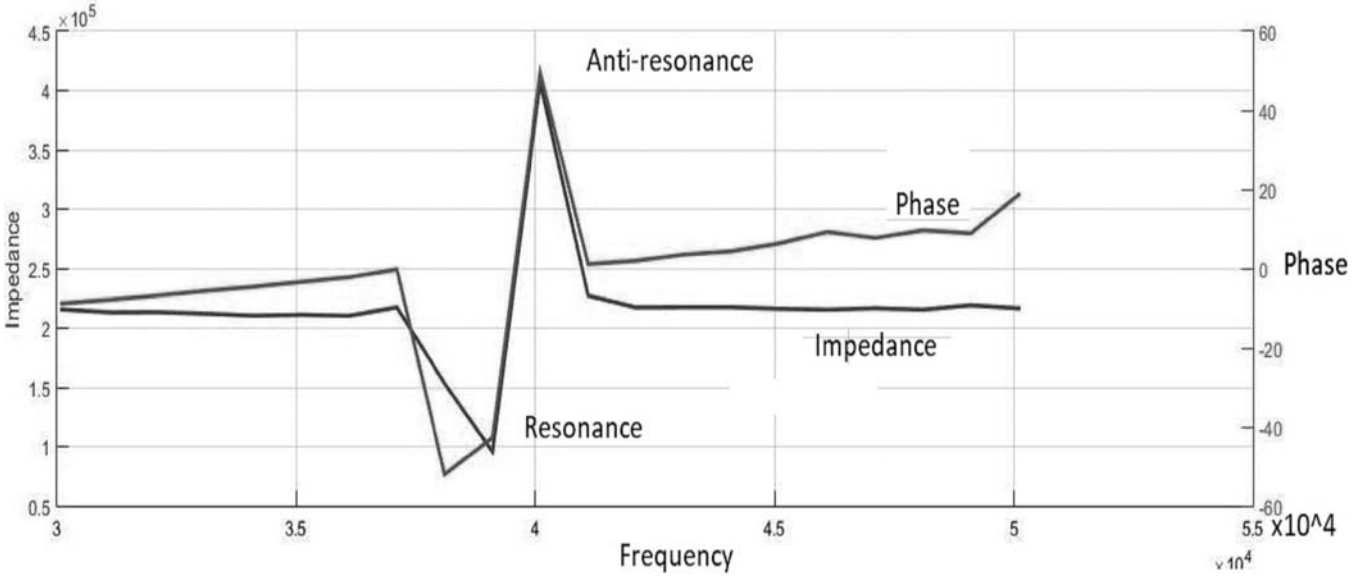

Fig. 2 Variation of Impedance (Z) and Phase (θ) with frequency

anti-resonance, the ultrasonic elements first approaches the minimum impedance, at which it vibrate most readily and the frequency for which it vibrate at maximum intensity known as resonance frequency. As excitation frequency is further increased impedance increases to the maximum value and frequency is called as anti-resonance frequency[5,7,8].

It is clearly seen that the transducer has negative phase in its resonance this predicts the capacitive behaviour of transducer and at the anti-resonance the transducer shows the positive phase change *i.e.* the transducer exhibits purely inductive behaviour. The resonance frequency for which the transducer vibrates at its maximum intensity is 39.1 kHz and the impedance is 95.6 *kΩ*,

where as the anti-resonance is at 40.1 kHz and the impedance at anti-resonance is 406 *kΩ*.

References

1 **Arnold F.J., Gonçalves M.S., Roger L.L.B.** and **Mühlen S.S.**, Electrical impedance of piezoelectric ceramics under acoustic loads, **12** (2014) 48-54.

2 **Brennan, S.**, Measuring loudspeaker impedance profile using the AD5933, Application Note AN-843, *Analog Devices*, (2007) 1-12. http://www.analog.com/media/en/technical-documentation/application-notes/236037846AN_843.pdf

3 1 MSPS 12-bit impedance converter, network analyzer, *Analog Devices*, (2011) 1-44. http://d1.amobbs.com/bbs_upload782111/files_25/ourdev_530698.pdf

4 **Bogatin E., Signal**, Power Integrity-Simplified 2nd Edition, *Prentice Hall, Michigan*, (2009) 92-97.

5 **Lee W.** and **Sung C.**, Sweep type resonant frequency tracking for dual ultrasonic transducers under water, *Int. J. Elect. Electron. Data Comm.*, **5** (2017) 23-25.

6 **Lis, W.** and **Schmidt J.**, Measuring the impedance of Ultrasonic transducers, *Hydroacoust*, **7** (2004) 143-148.

7 **Kuang, Y., Jin Y., Cochran S.** and **Huang Z.**, Resonance tracking and vibration stabilization for high power ultrasonic transducers, *Ultrasonics*, **54** (2014) 187-194.

8 **Zhang H., Wang F., Zhang D., Wang L., Hou Y.** and **Xi T.**, A new automatic resonance frequency tracking method for piezoelectric ultrasonic transducers used in thermosonic wire bonding, **235** (2015) 140-150.

J. Pure Appl. Ultrason. 40 (2018) p. 91-92

Ph.D. Thesis Summary

Investigation of Ultrasonic and Thermophysical Properties for Some Advanced Materials

(Awarded in 2017 by Amity University, Noida to Dr. Vyoma Bhalla, Department of Electronics & Communication Engineering, Amity School of Engineering & Technology Delhi)

The main aim of the thesis entitled "Investigation of Ultrasonic and Thermophysical Properties for Some Advanced Materials" is theoretical investigation of the elastic, mechanical, ultrasonic and thermophysical characterization of certain advanced materials such as rare-earth monopnictides and monochalcogenides. Further, the experimental analysis of thermal conductivity and ultrasonic velocity of nanofluid dispersion solution of titanium dioxide and propylene glycol has been conducted.

The advanced materials such as rare-earth compounds have drawn tremendous interest due to their remarkable structural, elastic, electronic, magnetic, phonon and thermal properties and are of technological relevance. These materials crystallize into simple NaCl-structure making them promising candidates for both experimental and theoretical analysis. The existence of single crystal of chosen materials became one of the most important reasons for the theoretical analysis of the rare-earth compounds. Recently, the considerable attention on these materials has further grown after it has been demonstrated that some rare-earth compounds can be grown epitaxially on III-V semiconductors. It has open up a way for their application in material producing industry, infrared detectors, optoelectronic devices, spintronics and research fields, etc.The study was performed on the temperature reliant characteristics of number of rare-earth monopnictides and monochalcogenides in the range of temperature 0-500K following theoretical approach which is based on Coulomb and Born-Mayer potential upto second-nearest neighbours (vander Waals' forces of interaction is not considered here). A computer program is developed in MATLAB based on the scheme of continuum approximation. The entire computations were based on the fact that there will be no modification observed in the crystal structure on varying the temperature till the melting point of the chosen materials under study. We report for the first time the temperature dependent elastic behaviour of these solids using simple Coulomb and Born-Mayer interionic potential approach. It is in relevance to the force shell model and is appropriate for explaining the anharmonic properties of several compounds such as second-order elastic constants (SOECs) and their combinations, elastic moduli, and pressure derivatives of elastic moduli, etc. Further, for studying the internal structure and inherent properties of solids, the theoretical ultrasonic attenuation technique is being used. The results of present investigation have been analysed in correlation with mechanical and thermophysical properties of the similar materials due to the absence of measured data following the similar approach wherever relevant. These analyses for the materials under study have been performed due to their several fascinating properties and several practical applications in the field of electro-optic components, non-linear optics, composites lasers, glass manufacturing, phosphor lasers and electronics and spintronics.

In all, the results presented in this theoretical work on the temperature dependent study of elastic, mechanical, thermal and ultrasonic properties of rare earth monopnictides and monochalcogenides are of primary importance. The data provides a better understanding of these materials for further investigation into potential industrial applications such asNDT of materials, thermal insulators and conductors, high temperature materials, spintronics, device fabrication, electronic industry and scientific research and experimentation. The preliminary results obtained

in the present work can be used for further experimental investigation with the pulse echo overlap (PEO) technique for ultrasonic measurements, and with conventional analytical techniques such as polarizing microscopy, X-ray diffraction (XRD), surface tension analysis, solid-state nuclear magnetic resonance (NMR), scanning electron microscopy (SEM) and transmission electron microscopy (TEM) and offers a new dimension, to further study the effect of attenuation on the grain size, edge and screw dislocations, etc., and its applications.

It would be interesting to extend ultrasonic measurements on REPn and RECh at low temperatures for the study of ultrasonic attenuation due to electron-phonon interaction (EPI) if some electrons are available in valence band. From a basic, research point of view it would be very valuable to measure variations in elastic properties with applied electric and magnetic fields in these crystals. In future applications, the typical properties of these monopnictides and monochalcogenides will be highly utilized in fabrication of hybrid devices such as hybrid car engines, high energy spectroscopy, laser sources, television screens, electronic industries, etc.

Further, the temperature dependent experimental study was performed. For this a colloidal mixture of nano-sized (<100 nm) TiO_2 (p-25) particles dispersed in a base fluid propylene glycol was formulated by the two-step method. The volume fractions of nanoparticles used were 0.1% and 0.50% for preparing the nanofluids. The average sizes, size distribution and surface morphology for the characterization of nanoparticles at different magnification have been determined using FESEM. The thermal conductivity and ultrasonic velocity of the prepared nanofluids at different concentration were experimentally studied in the temperature range of 20-80°C.Results show that thermal conductivity increases whereas the ultrasonic velocity decreases with increasing temperature. The ultrasonic investigation confirms the enhancement of thermal conductivity of nanofluids as reported in literature. The thermal conductivity of TiO_2/PG based nanofluids with particle volume fraction of 0.1% and 0.5% were investigated experimentally at different temperatures. The results show that the thermal conductivity increases with particle volume fraction and temperature. This parameter is important for the high temperature applications of the chosen nanofluids. Ultrasonic velocity decreases with the increase in temperature and concentration due to increase in density and compressibility. The acoustical study performed using ultrasonic wave propagation indicates the strong dependence of nanoparticle-fluid interaction on temperature and concentration. The exceptional property of thermal conductivity of nanoparticles considerably enhances the convective heat transfer coefficient in microchannels, industrial cooling applications and food processing industry.

Journal of Pure and Applied Ultrasonics

(INDEXED IN: Indian Citation Index, Google Scholar, i-Scholar, UGC List)

INFORMATION FOR AUTHORS

1. Type of Contribution

JOURNAL OF PURE AND APPLIED ULTRASONICS welcomes contributions on all aspects of ultrasonics including ultrasonic studies in medical ultrasonics, NDT, underwater, transducers, materials & devices and any other related topic. Contributions should fall into one of the following classes.

Paper - These should be on original research work contributing to scientific developments. They should be written with a wide readership in mind and should emphasize the significance of the work.

Reviews and Articles - Includes critical reviews and survey articles.

Research and Technical notes - These should be short descriptions of new techniques, applications, instruments and components.

Letters to the editor - Letters will be published on points arising out of published articles and papers and on questions of opinion.

Miscellaneous - Miscellaneous contributions such as studies, interpretive and tutorial articles, conference reports and news items are also accepted. Recommended contribution lengths are: Papers 2000-4000 words. Reviews and Surveys 2000-5000 words; Conference Reports 500-1500 words; News Items, Research and Technical Notes up to 1000 words.

2. Manuscripts

Manuscripts should be typed on one side of the paper in double spacing with 25 mm margin on all sides of A4 size paper. A soft copy of the manuscript in MS WORD for text and MS EXCEL for illustrations and a PDF file thereof may be sent by e-mail or CD/ DVD. Colour images should be formatted as JPEG files. Figures submitted in colour would be published in colour. Colour should be avoided unless it is required in order to convey a message or serve a purpose in the image.

Title - Titles should be short and indicate the nature of the contribution.

Abstract - An abstract of 100-200 words should be provided on the title page of paper and review article. This should indicate the full scope of the contribution and include the principal conclusions.

Mathematics - Mathematical expressions should be arranged to occupy the minimum number of lines consistent with clarity e.g., $(x^2+y^2)/(x-y)^{1/2}$.

Illustration - The line illustrations along with captions should be clearly drawn with black Indian ink. Figures in Excel are preferred.

References - References should be referred to in the text by number only. The reference number should be given as superscript. The corresponding reference shall contain the following information in order; names and initials of author (s)(bold), title of the work, journal or book title (italic), volume number (bold), year of publication in brackets, page number, e.g., **Kumar S. and Furuhashi H.,** Anisotropic divergence controlled ultrasonic transmitter array for three dimensional range imaging, *J. Pure Appl. Ultrason.,* **38** (2016) 49-57.

Units and Abbreviations - Authors should use SI units wherever possible.